# **Understanding Boreal Summer UTLS Water Vapor Variations in Monsoon Regions: A Lagrangian Perspective**

Hongyue Wang<sup>1</sup>, Mijeong Park<sup>2</sup>, Mengchu Tao<sup>3</sup>, Cristina Peña-Ortiz<sup>4</sup>, Nuria Pilar Plaza<sup>5</sup>, Felix Ploeger<sup>1,6</sup>, and Paul Konopka<sup>1</sup>

**Correspondence:** Paul Konopka (p.konopka@fz-juelich.de)

Abstract. Water vapor in the upper troposphere and lower stratosphere plays a crucial role in climate feedback, affecting radiation, chemistry, and atmospheric dynamics. This study presents simplified Lagrangian reconstructions of stratospheric water vapor satellite observations from SAGE III/ISS and MLS instruments, to improve the understanding of moist anomalies in the Asian and North American monsoons and to identify the key factors contributing to model biases. Our findings show that while both SAGE III/ISS and MLS capture similar spatial patterns, SAGE III/ISS shows higher local values. The performance of Lagrangian reconstructions significantly improves with the size of trajectory ensembles but exhibits a general dry bias across the tropics. However, the reconstruction represents the Asian monsoon moist anomaly well, particularly above the tropopause, whereas it fails to capture the North American monsoon anomaly. The main dehydration, region as diagnosed from trajectories, indicates that water vapor is predominantly controlled by local temperatures near the tropopause in the Asian Monsoon. North American monsoon is largely influenced by long-range transport from dehydrated regions over Southeast Asia, while moist air masses are primarily controlled by local dehydration. Hence, the limited performance of the reconstruction for the North American monsoon is potentially linked to an underestimation of local convection or uncertainty in long-range transport. Additionally, dry bias in reconstruction over the Asian monsoon shows a positive correlation with intensity of convection particularly in the western sector, suggesting that an underestimation of moistening due to convective ice injection may play a role in this region.

## 1 Introduction

Stratospheric water vapor  $(H_2O)$  is a potent greenhouse gas that can significantly amplify warming of the global temperature due to its strong radiative effects and long residence time (Solomon et al., 2010; Riese et al., 2012). The amount of water vapor entering the stratosphere is primarily controlled by the freeze-drying process—the dehydration of moist tropospheric air as it ascends through the cold point tropopause (Brewer, 1949; Randel and Park, 2019; Smith et al., 2021). This freeze-drying occurs

<sup>&</sup>lt;sup>1</sup>Institute of Climate and Energy Systems, Stratosphere (ICE-4), Forschungszentrum Jülich, 52428 Jülich, Germany

<sup>&</sup>lt;sup>2</sup>U.S. National Science Foundation National Center for Atmospheric Research (NSF NCAR), Boulder, CO 80307, USA

<sup>&</sup>lt;sup>3</sup>Carbon Neutrality Research Center, Institute of Atmospheric Physics, Chinese Academy of Sciences, Beijing 100029, China

<sup>&</sup>lt;sup>4</sup>Departamento de Sistemas Físicos, Químicos y Naturales, Universidad Pablo de Olavide, 41013 Seville, Spain

<sup>&</sup>lt;sup>5</sup>Centro de Investigaciones sobre Desertificación, Consejo Superior de Investigaciones Científicas (CIDE-CSIC), 46113 Moncada, Valencia, Spain

<sup>&</sup>lt;sup>6</sup>Institute for Atmospheric and Environmental Research, University of Wuppertal, 42119 Wuppertal, Germany

mainly in the tropical tropopause layer (Fueglistaler et al., 2009), where air masses ascend slowly (diabatically) from the level of main convective outflow into the stratosphere over weeks to months. During this ascend, air parcels travel horizontally over thousands of kilometers and likely sample the coldest tropopause regions (the 'cold trap') (Holton and Gettelman, 2001). On the other hand, water vapor and ice can be directly injected into the Upper Troposphere and Lower Stratosphere (UTLS) through deep, overshooting convection, and it has been argued that this process happens frequently in the tropics and over North America during boreal summer (Homeyer et al., 2023). This convection-driven transport is characterized by rapid vertical updrafts near convective centers, occurring in the timescales on the order of minutes (Jorgensen and Lemone, 1989; Schwartz et al., 2013). However, the extent to which this hydration process affects stratospheric water vapor remains under debate (Randel et al., 2012; Avery et al., 2017; Ueyama et al., 2020; Jensen et al., 2020; Ueyama et al., 2023; Homeyer et al., 2023; Konopka et al., 2023).

During boreal summer, enhanced water vapor is observed in the UTLS over regions influenced by the Asian Summer Monsoon (ASM) and North American Monsoon (NAM) (Ploeger et al., 2013; Park et al., 2021; Clemens et al., 2022). This enhancement is often attributed to intense convection, which can transport water vapor directly into the UTLS (Fu et al., 2006; Yu et al., 2020). Besides localized convection, seasonal variations in tropical tropopause temperatures play a key role in modulating UTLS water vapor levels, with peak concentrations occurring in boreal summer and autumn (Randel et al., 2004; Tao et al., 2023). In particular, the ASM has been recognized as a major contributor to stratospheric water vapor, accounting for ~15% of the tropical stratospheric water vapor anomaly and ~30% of the summertime NH extratropical water vapor maximum (Bannister et al., 2004; Wright and Gille, 2011; Rolf et al., 2018; Nützel et al., 2019). These observational studies, however, have limitations in understanding the physical processes that are driving the enhancement in water vapor concentrations over the monsoon regions. Understanding those mechanisms and the interactions between regional convection, large-scale transport and thermodynamic conditions is the key to predict the potential impact of stratospheric water vapor on our climate.

In this study, our goal is to evaluate the role of the freeze-drying mechanism in the large-scale temperature and wind fields for the enhancement of stratospheric water vapor over the ASM and NAM regions from a Lagrangian perspective. Lagrangian methods track the history of air parcels (their trajectories) and reconstruct stratospheric water vapor based on the coldest temperature encountered along these trajectories, commonly referred to as the Lagrangian cold points (LCP) temperature (Fueglistaler et al., 2005). By capturing the cumulative effects of large-scale transport and temperature variability over timescales ranging from days to months, Lagrangian methods have been successfully used to reproduce UTLS water vapor anomalies (Mote et al., 1995; Fueglistaler and Haynes, 2005; Liu et al., 2010; Schoeberl and Dessler, 2011; Smith et al., 2021). We firstly conduct Lagrangian back-trajectory simulations utilizing the trajectory module of the Chemical Lagrangian Model of the Stratosphere (CLaMS) (McKenna et al., 2002), to reconstruct satellite observations by the Stratospheric Aerosol and Gas Experiment III on the International Space Station (SAGE III/ISS) Davis et al. (2021) Version 5.3 and Aura Microwave Limb Sounder (MLS) Version 5.0 Lambert et al. (2017). These Lagrangian reconstructions are driven by the fifth generation European Centre for Medium-Range Weather Forecasts atmospheric reanalysis (ERA5) (Hersbach et al., 2020). We then assess the performance of the Lagrangian reconstruction in capturing boreal summer UTLS water vapor distributions by comparing simulation results to the satellite observations. Additionally, we compare the monsoon regions to the deep tropics, where similar Lagrangian

reconstructions were successfully applied in the past (Fueglistaler et al., 2005; Hasebe and Noguchi, 2016; Smith et al., 2021). SAGE III/ISS is utilized for its higher vertical resolution (2 km compared to ~3 km in MLS near the UTLS region (Read et al., 2007)), providing a more detailed representation of water vapor vertical structures within the monsoon anticyclones. In addition, MLS provides daily global coverage and has widely been used in numerous studies on stratospheric water vapor Mote et al. (1995); Liu et al. (2010); Nützel et al. (2019). Furthermore, we analyze the spatial and temporal locations of the LCPs in relation to observed water vapor distributions within the monsoon regions. We also investigate the potential factors contributing to discrepancies between the Lagrangian reconstructions and observations, with a particular focus on deep convection, which is only partly resolved in ERA5 meteorology. As a proxy for the intensity of convection, we use Outgoing Longwave Radiation (OLR) derived from satellite observations (Kumar and Krishnan, 2005).

The main research questions explored in this paper are: (i) How well can stratospheric water vapor mixing ratios in the ASM and NAM as observed by SAGE III/ISS and MLS be reconstructed using a simplified Lagrangian modelling method, especially in comparison to the deep tropics? (ii) Are the moisture anomalies observed within the ASM and NAM anticyclones locally or remotely controlled by the LCPs and which regions are most critical? (iii) Are model biases in the reconstruction related to particular processes (e.g., convection)?

This paper is organized as follows: Section 2 presents the datasets and model used, and describes the reconstruction method. Section 3 outlines our main results, including the assessment of Lagrangian water vapor reconstructions and the analysis of LCPs. Section 4 discusses the potential causes of biases in the Lagrangian reconstruction results and relations to convection. Section 5 provides the conclusions.

## 2 Data and Method

# 5 2.1 Satellite observations

## 2.1.1 MLS

85

65

The Microwave Limb Sounder (MLS) instrument on the Aura satellite Waters et al. (2006) has been providing global measurements of various atmospheric constituents since August 2004, including water vapor, ozone, carbon monoxide, sulfur dioxide, nitric acid, and nitrous oxide profiles using radiances from the nearest limb scan (https://www.earthdata.nasa.gov/learn/find-data/near-real-time/mls). MLS provides a comparatively high sampling with about 3500 measurement profiles per day. Here, we use version 5.0 (v5.0) data, which provides water vapor profiles in 2.1–3.5 km vertical resolution (Lambert et al., 2017), with ~3.0 km resolution in lower stratosphere (Read et al., 2007). We focus on water vapor measurements for the month of August from 2017 to 2019 in the subtropical regions (35°S–35°N). The MLS water vapor profiles are then gridded in 10°× 20°(latitude × longitude) horizontal grids. For more details on MLS water vapor and the retrieval technique see Livesey et al. (2020).

## 2.1.2 SAGE III/ISS

The Stratospheric Aerosol and Gas Experiment III on the International Space Station (SAGE III/ISS) was launched on February 19, 2017 Cisewski et al. (2014) and has been providing measurements of aerosol, water vapor and ozone between 70°S and 70°N latitude using solar occultation, lunar occultation and limb scattering. We use Level 2 (L2) Solar Event Species Profiles (HDF5) Version 5.3 (v5.3) data product (https://asdc.larc.nasa.gov/project/SAGEAccording to Davis et al. (2021), there is good agreement between SAGE III/ISS v5.1 and MLS v5.0 water vapor measurements in the stratosphere, with SAGE III/ISS v5.1 being drier than MLS (~0.5 ppmv or 10%) in the 15–35 km altitude range. However, SAGE III/ISS v5.1 profiles were affected by low-quality data due to aerosol and cloud-related interferences (Park et al., 2021; Davis et al., 2021). These issues—such as failed retrievals and increased sensitivity to elevated aerosol loading—were largely mitigated in version 5.2 and subsequent versions, as noted in the SAGE III/ISS Data Products User's Guide (https://asdc.larc.nasa.gov/documents/sageiii-iss/guide/DPUG\_G3B\_v05.30.pdf).

We focus on the water vapor measurements in the month of August for 2017-2022 in the subtropics (35°S–35°N). We added three more years (2020–2022) of the SAGE III/ISS measurements to increase spatial coverage of SAGE III/ISS water vapor. Comparison of the horizontal distributions of SAGE III/ISS water vapor for the 2017–2019 and 2017–2022 periods results in no significant differences and does not affect the results of our study. The water vapor profiles provided by SAGE III/ISS v5.3 product are originally retrieved on a 1.0 km grid and interpolated on a 0.5 km grid from 0.5–60.0 km in altitude. In this study, we perform a 1-2-1 vertical smoothing on all SAGE III/ISS water vapor profiles on a 0.5 km grid following Davis et al. (2021), resulting in a final vertical resolution of 2 km. The profiles are presented in units of number density. We convert the units into mixing ratio using temperature and pressure profiles from the Modern-Era Retrospective analysis for Research and Applications, Version 2 (MERRA-2). Binned data used here for presenting horizontal distributions are gridded with resolution of 10°× 20°(latitude × longitude), requiring at least 5 profiles in each bin. We follow the similar procedure described in Park et al. (2021), where SAGE III/ISS v5.1 was used.

## 2.2 OLR

100

105

115

We use daily mean outgoing longwave radiation (OLR) as a proxy for deep convection. The OLR data is obtained from the National Oceanic and Atmospheric Administration (NOAA) Climate Prediction Center (CPC) (https://psl.noaa.gov/data/gridded/data.cpc\_blended\_olr-2.5deg.html). The CPC blended OLR Version 1 dataset is constructed by blending the level 2 OLR retrievals from NASA's Cloud and Earth Radiant Energy System broadband measurements, NOAA/NESDIS Hyperspectral measurements, and High-resolution Infrared Radiation Sounder measurements. The gridded daily OLR from NOAA covers the period from 1991 to the most recent date, on a 2.5°× 2.5°(latitude × longitude) global grid. We subtract the monthly averages at each grid point to obtain the OLR anomalies. The OLR indices used in this study are calculated by averaging the OLR anomalies within specific regions. For the ASM, the indices are defined as follows: (i) OLR-West: 20–30°N, 50–80°E, (ii) OLR-East: 20–30°N, 80–110°E. This separation of convective regions in the ASM follows Randel et al. (2015), and our results are not sensitive to the exact separation longitude. For the OLR values shown in Fig. 8, we use the original values

instead of anomalies. Note that, while OLR is a commonly used proxy for convective intensity, it has limitations in identifying deep convection due to its reliance on infrared measurements. These measurements can underestimate cloud-top temperatures, particularly over land and for aged anvil clouds (Liu et al., 2007).

## 2.3 Models

135

140

## 2.3.1 CLaMS trajectory module

Chemical Lagrangian Model of the Stratosphere (CLaMS) is an advanced modeling framework designed for simulating the transport and chemical processes in the atmosphere (McKenna et al., 2002; Konopka et al., 2022). It employs a Lagrangian approach, where air parcels are tracked individually, allowing for a detailed and accurate representation of atmospheric dynamics and chemistry. For this study, we use the trajectory module of CLaMS 2.0, which specifically focuses on the trajectory calculations of air parcels (https://clams.icg.kfa-juelich.de/CLaMS/traj). The driving meteorological fields for these simulations are from ERA5, with 1°× 1° (latitude × longitude) horizontal resolution, 137 vertical hybrid layers and 6-hour time interval (Hersbach et al., 2020). We perform 180-day back-trajectory calculations for air parcels, with each air parcel launched from the precise spatial location and time corresponding to the satellite data profiles within the tropics. For each August from 2017 to 2022, SAGE III/ISS provides 149, 203, and 2292 profiles for the ASM, NAM, and tropics, respectively. For each August from 2017 to 2019, MLS provides 7801, 10,223, and 126,981 profiles for the ASM, NAM, and tropics, respectively. Taking the ASM as an example, the number of calculated trajectories is determined by  $149 \times 10$  (profiles × levels) for the LAG single experiment (for the definition of the different model experiments see Sect. 2.3.2) and  $149 \times 10 \times 51$  (profiles × levels × ensemble trajectories) for the LAG experiment. Accordingly, the total number of calculated trajectories for LAG single is 1490 for the ASM, 2030 for the NAM, and 22,920 for the tropics, while for LAG, these values increase to 75,990, 103,530, and 1,168,920, respectively. Similarly, for MLS the number of trajectories for LAG single is 39 005 for the ASM, 51 115 for the NAM, and 634 905 for the entire deep tropics, while for the LAG experiment these values are multiplied by 51, resulting in significantly larger trajectory ensembles.

## 2.3.2 Water vapor reconstruction

We reconstruct water vapor concentrations by identifying the cold point temperature. From the local perspective, cold points are the lowest temperatures observed along local vertical profiles. From the Lagrangian perspective, the cold points are defined as the minimum temperatures encountered along the back-trajectories of air parcels, after interpolating the ERA5 temperature and pressure data along the back-trajectories. The reconstructed stratospheric water vapor concentrations are calculated using the following formulas:  $H_2O_{\rm ppmv} = 1.0 \times 10^6 \cdot e_{\rm sat}/(P-e_{\rm sat})$ , where the saturation vapor pressure  $e_{\rm sat}$  is given by  $e_{\rm sat} = 10^{\left(\frac{A}{CPT} + B\right)}/100$ . Here, A = -2663.5, B = 12.537, CPT is the cold point temperature in K, and P is the pressure in hPa (Sonntag, 1994).

In the following, we present results from our experiments based on three types of reconstructions: LOC, LAG\_single and LAG. (a) LOC uses the minimum temperatures along the vertical profiles associated with SAGE III/ISS, which are derived

from MERRA-2 reanalysis. These minimum values are treated as local cold point temperatures (CPTs) and are used in the previously introduced equations to calculate the reconstructions. (b) For LAG single, back-trajectory simulations are initialized on each measurement point in the UTLS, using the observed altitude, longitude, and latitude of that point. Upon obtaining the trajectories, we then find the LCP temperatures to calculate the reconstructions at all the observation points. For the SAGE III/ISS dataset, we set the starting points at altitudes ranging from 14.0 km to 21.0 km, with a 0.5 km interval. For the MLS dataset, we convert pressure to geopotential height then used the one closest to the SAGE III/ISS altitude. (c) For LAG, each measurement point is reconstructed using an even larger ensemble of trajectories by initiating 50 additional starting points vertically spaced at 10-meter intervals above and below the observation point. This results in a total of 51 trajectories, including the original one at the observation point. The reconstruction is then based on the ensemble of these back-trajectories. For example, if the observation point is at 16.0 km (as in the SAGE III/ISS dataset), we set the starting point at 16.0 km and add 50 more points from 15.25 km to 16.25 km, with 0.01 km (10 meters) interval. The final reconstruction value for this observation point is calculated by averaging the reconstruction values from all 51 back-trajectories, to enhance the vertical sampling around the original observation point. The final reconstruction value is obtained by averaging all the reconstructed back-trajectories. This dense sampling enhances the vertical resolution of the reconstruction. We specifically increase vertical sampling because vertical wind shear generally leads to stronger redistribution of air parcels compared to horizontal shear. As air parcels move, they are stretched into thin and horizontally extended layers due to quasi-isentropic flow. This horizontal spreading gradually dilutes the parcels and lessens the necessity for denser horizontal sampling. Also, given the vertical resolution of MLS and SAGE III/ISS data (3 km and 2 km, respectively), it is more important to increase the vertical sampling in our trajectory calculations to better reconstruct the water vapor mixing ratios. For further details of these processes, refer to Haynes and Anglade (1997), which explains how differential advection in the atmosphere drives vertical mixing and stretching of air parcels.

All the back-trajectories are categorized into two groups: those that cross the tropopause are referred to as Troposphere-to-Stratosphere Transport (TST), and those that do not are referred to as non-TST. TST trajectories are defined as those with starting points (or observation points) located above 370 K potential temperature and traced back to below 340 K potential temperature. For TST trajectories, the reconstructed water vapor concentrations are calculated using the LCP temperatures. For non-TST trajectories, the reconstructed values are defined as the smaller of the two: the saturation mixing ratios based on LCP temperatures, and the climatological water vapor concentrations from MLS at the earliest back-trajectory endpoints.

## 3 Results

165

175

## 3.1 Performance of Lagrangian water vapor reconstruction

#### 180 3.1.1 Spatial distributions

Both the ASM and NAM regions show enhanced water vapor mixing ratios based on satellite observations during boreal summer. Figures 1a and 1b show horizontal distributions of water vapor in August at ~16.5 km (around 100 hPa pressure level

or 380 K potential temperature level) based on SAGE III/ISS and MLS satellite observations, respectively. The distributions from both satellite datasets show consistent spatial patterns, with the maxima located over the ASM (15°–35°N, 50°–150°E) and NAM (10°–35°N, 160°–80°W). The high values from SAGE III/ISS (exceeding 7 ppmv) are higher than the values from MLS (5–6 ppmv). Figure 1c and 1d present reconstructed water vapor derived from ensemble trajectories (Experiment LAG), where more than 80% of the trajectories are classified as TST (Sect. 2.3.2), based on the profiles from SAGE III/ISS and MLS, respectively. Overall, the reconstructions exhibit a noticeable dry bias across the entire tropics compared to the observations. Concerning the spatial patterns, however, the water vapor distributions reconstructed from trajectories for the two satellite datasets are similar, in particular showing elevated mixing ratios above the ASM, similar as in the satellite observations. While the elevated water vapor mixing ratios in the ASM are captured, the observed moist anomaly in the NAM is not reconstructed from trajectories.

185

190

195

200

210

215

The observed anomalies from SAGE III/ISS are ~1–2 ppmv over the ASM and NAM (Fig. 1e), which is higher than the those from the MLS (~1 ppmv) as shown in Fig. 1f. Compared to the observations, the reconstruction successfully captures the water vapor anomalies over the ASM (1–2 ppmv), covering smaller area. However, the reconstruction over the NAM shows an increase of less than 0.5 ppmv in water vapor concentrations, with the maximum located near the equator.

Figure 2 analyzes the vertical structure of the observed and reconstructed water vapor profiles, averaged over the three regions of interest: tropics, ASM, and NAM. All water vapor profiles show a decrease in concentration from the troposphere to the UTLS region. The variability in water vapor is greater in the troposphere than in the stratosphere. The reconstructed profiles partially capture these distinct characteristics of water vapor in both the troposphere and stratosphere, in terms of both concentration and variability.

In the tropics (Fig. 2a–b), the cold point tropopause and the lapse rate tropopause are located at 16.7 km (cyan dashed lines) and 15.7 km (yellow dashed lines), respectively. Below the lapse rate tropopause, the reconstructed profiles (blue lines) based on SAGE III/ISS show maximum dry biases of -2.3  $\pm$  2.5 ppmv at 15.5 km, while MLS-based reconstructions exhibit biases of -1.5  $\pm$  1.5 ppmv at ~15.1 km. Within the tropical tropopause layer (between the cold point and lapse rate tropopauses), both the magnitude and variability of the dry biases gradually decrease with increasing altitude. Above the cold point tropopause, the dry biases decrease to -1.7  $\pm$  0.7 ppmv (-34%  $\pm$  14%) at 17.0 km based on SAGE III/ISS, and to -0.8  $\pm$  0.6 ppmv (-21%  $\pm$  15%) at ~17.4 km based on MLS. Similar dry biases have been reported by Liu et al. (2010), who found that stratospheric water vapor predictions based on the saturation mixing ratio at the Lagrangian dry point of trajectories exhibit dry biases of up to -50%  $\pm$  10%, which they attributed to missing cloud microphysics. Above 19.0 km, the biases in the reconstructions are 1–2 ppmv smaller when both TST and non-TST trajectories are considered (Fig. S1), compared to when only TST trajectories are used (Fig. 2). The black diamonds in Fig. S1 represent the percentage of TST trajectories relative to the total number of trajectories, indicating that non-TST trajectories account for more than 95% above 19.0 km. This suggests that water vapor concentrations in the higher stratosphere align more closely with climatological values and less with direct transport from the upper troposphere within 180 days.

In monsoon regions, the main structures of both observed and reconstructed profiles are similar to those in the tropics, though there are some noticeable differences. From the observed profiles, UTLS water vapor concentrations in monsoon regions are

higher than in the entire tropics, especially below the lapse rate tropopause. The anomalies of observations, compared to the average in the tropics, reach 4.5 ppmv at 16.5 km for the ASM (Fig. 2c) and 1.5 ppmv for the NAM (Fig. 2c), as derived from SAGE III/ISS observations.

220

225

230

245

250

In the ASM region, the tropopause layer is higher and thinner (16.6–17.1 km) compared to that in the tropics. For the reconstructions based on SAGE III/ISS, the reconstructed ASM profiles have substantial dry biases below the lapse rate tropopause, up to  $-4.9 \pm 4.2$  ppmv at 15.5 km (Fig. 2c-d). However, these biases gradually decrease with altitude, reducing to  $-1.7 \pm 0.8$ ppmv at 17.5 km, consistent with the bias levels seen in the tropics. To further assess the vertical performance of the reconstruction, we compare the reconstructed ASM anomalies relative to the entire tropics. At 15.5 km, the SAGE-based reconstructions capture approximately one-third of the observed anomalies (Fig. 2b; right sub-panels). The agreement improves significantly with altitude: at 16.5 km, the reconstructed anomalies account for over two-thirds of the observed values, and above this level, the reconstructions approach even closer agreement. Similar results are also reflected in the MLS-based reconstructions (Fig. 2e; right sub-panels). This shows that the Lagrangian reconstruction method performs reliably above tropopause levels. The consistent behaviour of the reconstruction in the ASM compared to the tropics further suggests that stratospheric water vapor above the ASM is primarily governed by the mechanisms-freeze-drying in the large-scale temperature field ('advectioncondensation' paradigm, see Liu et al., 2010)—as in the tropics. In contrast, at lower altitudes in the troposphere, water vapor is likely more strongly influenced by other processes such as deep convection. Consistent with our findings, Plaza et al. (2021) showed that while convection can moisten the upper troposphere, its signature could be erased by subsequent dehydration at higher altitudes. As a result, convection plays a limited role in determining water vapor concentrations in the lower stratosphere of monsoon regions, whereas small-scale mixing appears to be a more dominant contributor.

In the NAM, the tropopause layer (15.6–16.5 km) is slightly lower and thinner compared to that in the tropics (Fig. 2c and 2f). As the altitude increases, the bias profile based on SAGE III/ISS decreases more slowly than in the ASM, with a remaining bias of  $-1.8 \pm 1.2$  ppmv at 17.0 km within the stratosphere (Fig. 2c). Moreover, the fraction of the observed anomaly captured by the reconstruction is considerably lower in the NAM compared to both the ASM and the tropics (Fig. 2c and 2f; right subpanels). The distinct structure of the tropopause layer and the corresponding reconstruction performance in the NAM suggest that considering only the freeze-drying effect by advection through the large-scale temperature field (as represented in the Lagrangian reconstruction method) is insufficient to explain the moist anomaly in the NAM region. Hence, further processes like convection, mixing, and ice microphysics are likely to play a more significant role in stratospheric water vapor variability in the NAM.

Comparing the profiles from SAGE III/ISS (left) with those from MLS (right), the higher vertical resolution profiles from SAGE III/ISS show more strongly enhanced water vapor concentrations and clearer peak values in the UTLS for the three regions of focus, especially the ASM. The reconstructions based on SAGE III/ISS and MLS resemble each other. The SAGE III/ISS dataset, with its higher vertical resolution, captures more features of water vapor variations in the UTLS, while MLS may lose information due to lower vertical resolution. However, the limited and uneven sampling of SAGE III/ISS might restrict its ability to reveal spatial features, which could be the main reason for the slight differences between the reconstructions based on the two datasets.

## 3.1.2 Lagrangian reconstruction sensitivities

To assess the performance of the reconstructions from different experiments, we present the correlation coefficients between observed and reconstructed water vapor concentrations in Fig. 3. In addition to the Lagrangian reconstruction using cold point temperatures from ensemble trajectories (LAG) based on both SAGE III/ISS and MLS datasets, we also include the reconstruction using cold point temperatures from individual trajectories (LAG\_single) and the reconstruction using local cold point temperatures (LOC) only based on SAGE III/ISS profiles. This allows a direct comparison of the Lagrangian methods with the local perspective. Note that the x-axis in each plot shows the length of the backward period used for the trajectory calculations, thus the correlation coefficients for LOC remain constant.

The reconstructions from LAG exhibit the highest correlation with observations, followed by LAG\_single, while LOC shows the lowest correlation coefficients: -0.12 in the tropics, 0.07 in the ASM, and -0.17 in the NAM. As expected, using local cold point temperatures to determine stratospheric water vapor yields unreliable results (compare Fueglistaler et al., 2005). Similarly, smaller trajectory ensembles (LAG\_single) have limited accuracy, as trajectory reconstructions are highly sensitive to the initial air parcel position and small variations in wind and diabatic heating fields. By averaging over larger trajectory ensembles (LAG), the reconstruction becomes more robust and accurate, effectively capturing the inherent uncertainties in the system. For the results based on MLS and SAGE III/ISS, changing the dataset does not significantly affect reconstruction performance across the three regions. This suggests that the results based on SAGE III/ISS are generally representative and reliable for the purposes of this study, despite its lower horizontal and temporal sampling compared to MLS.

The reconstruction of water vapor using the Lagrangian method aims to find the minimum saturation mixing ratio along the trajectory, and therefore the backward time length of the simulation might influence the results. As shown in Fig. 3, all Lagrangian experiments display a consistent increasing trend in correlation coefficients as the backward calculation time increases. For instance, in LAG (SAGE III/ISS), the correlation coefficients for the ASM region increase from 0.53 (with a 60-day backward period) to 0.69 (with a 180-day backward period), and from 0.43 to 0.75 for the NAM. The most rapid increase occurs when extending the backward period from 60 to 120 days. These significant improvements in the reconstruction suggest that UTLS water vapor concentrations in August are partially influenced by processes from boreal spring or even winter, particularly at higher altitudes, where the time periods elapsed since air parcels had encountered their LCPs may be months. Such delayed influence is also well-known in the context of the atmospheric 'tape recorder', where water vapor anomalies imprinted at the cold point propagate upward due to the weak tropical upwelling (Mote et al., 1996). Within the ASM anticyclone, weak mixing allows this memory effect to be preserved along upward-moving trajectories, which is also referred to as 'upward spiraling' (Vogel et al., 2019).

In general, it is known that the Lagrangian temperature history is necessary to explain the dehydration process in the tropical tropopause layer and the observed dryness of the lower stratosphere (Fueglistaler et al., 2005). However, in the Northern hemisphere monsoon circulations the air masses are confined to some degree and it is not clear per se if dehydration and moistening processes are controlled more strongly by local processes (e.g., convection in the monsoons). To investigate this question, Fig. 4 shows correlations of the SAGE III/ISS and MLS water vapor values observed in UTLS against local cold point temperatures

and against LCP temperatures, respectively. Clearly, the correlation between observed water vapor concentrations and local cold point temperatures is very weak (Fig. 4a–c), and the saturation values calculated using local cold point temperatures (grey points) show large moist biases compared to observed values: 15.14 ppmv on average in the tropics, 6.16 ppmv in the ASM, and 13.48 ppmv in the NAM. In contrast, the correlations between water vapor concentrations and LCP temperatures are much stronger, ranging from 0.60 for the ASM based on the SAGE III/ISS dataset (Fig. 4e) to 0.78 for the NAM region (Fig. 4f). The reconstructed water vapor biases are also significantly reduces to ~1–2 ppmv (but dryer) on average for all regions.

Hence, we find a similarity between the monsoon regions and the deep tropics regarding the correlation between observed lower stratospheric water vapor mixing ratios and LCP temperatures, but not with local cold point temperatures derived from reanalysis. This suggests that dehydration in these regions is likely governed by non-local processes associated with large-scale transport. However, we note that overshooting convection—often considered a direct injection mechanism for water vapor into the lower stratosphere—is a sub-grid scale process not fully resolved in reanalysis. Therefore, using local cold point temperatures may underestimate the impact of such events, and the weak correlation with local temperatures might not entirely rule out the role of local processes in monsoon regions.

The regression lines for observations versus LCP temperatures (blue lines) in Fig. 4d–i all have smaller slopes than those for the saturation mixing ratios (grey lines), likely due to the influence of points above 19.0 km. Above this altitude, air is more likely to be well-mixed within the stratosphere, making water vapor concentrations less correlated with LCP temperature and more representative of climatological moisture conditions (Fig. S1). The ASM and NAM regression slopes from SAGE III/ISS (Fig. 4e–f) are closer to the saturation slopes, likely due to less sampling at high altitudes. Moreover, tracing air parcels back to the troposphere becomes more uncertain at higher altitudes, as longer back-trajectories introduce greater uncertainties in LCP determination.

## 3.2 Locations of the Lagrangian cold points

290

295

300

305

315

320

The Lagrangian reconstruction not only reproduces observed water vapor values but also traces the regions where dehydration occurred before reaching the observation points. Since dehydration events can take place weeks to months earlier, it is crucial to identify the dominant locations of these events and assess whether they are concentrated in specific regions or more broadly distributed across the tropics. Utilizing all back-trajectories (from experiment LAG), we trace the observations back to the specific locations of their LCPs. Given the large number of such trajectories, we calculate the spatial distribution of these locations using probability density functions (PDFs). The scatter plots of the locations of LCPs are shown in Fig. 5 (with colors denoting the reconstructed water vapor values), and the corresponding PDFs are presented in Fig. 6.

The results from the SAGE III/ISS and MLS datasets show similar patterns for both monsoon regions. In the ASM region (Fig. 5c–d), LCPs are spread across the 0–30°N zonal band, with most dehydration points situated in the ASM region and some extending into North Africa and North America. According to the PDF of the LCPs in Fig. 6c–d, most of the LCPs are located over India and the Bay of Bengal, around 10°–30°N, 70°–95°E, indicating the primary origin of reconstructed water vapor in the ASM. For the top 10% of the highest reconstructed water vapor concentrations (exceeding ~6 ppmv), the LCPs are concentrated in the same region (red contour lines), slightly displaced towards higher latitudes. This suggests that the increased

water vapor in the ASM, as determined by the reconstruction method, is primarily attributed to dehydration processes occurring in the vicinity of the monsoon over South Asia. According to Konopka et al. (2023), the 'dehydration carousel' mechanism within the ASM anticyclone plays a key role in shaping the distribution of water vapor entering the stratosphere, that is, while deep convection supplies moisture to the upper troposphere, the coldest regions near the monsoon's southern vicinity act as primary dehydration sites. Air parcels that undergo dehydration in these regions can later be transported within the anticyclone and ascend into the stratosphere, contributing to the observed high water vapor concentrations in the lower stratosphere.

The backward time length required for air parcels observed at 16.5km to reach these LCPs is shown in Fig. S2a–b, indicating that the dehydration processes occur over a timescale of days to weeks before the air parcels reach the observation points. Other LCPs, located further away and with lower reconstructed water vapor concentrations (1–5 ppmv), correspond to longer time periods (1–6 months) between the dehydration event and observation. While these air parcels with low water vapor are not the primary factor for the monsoon moist anomalies, their contribution to the water vapor budget highlights the need to extend the simulated backward time period, especially considering the improvements in correlation coefficients shown in Fig. 3. These findings reinforce the idea that the ASM anticyclone serves as a crucial transport pathway for air into the stratosphere, while dehydration near its vicinity regulates the amount of water vapor that ultimately enters the stratospheric circulation.

For the NAM region (Fig. 5e–f), a significant number of LCPs are observed across North America. Remarkably, the region of occurrence of LCPs extends throughout the 0–30°N zonal band even into southern Asia. The PDFs in Fig. 6e–f indicate that the primary dehydration center is in the ASM region, meaning that most air parcels in the NAM experienced dehydration in southern Asia. Focusing on the top 10% highest reconstructed water vapor concentrations (Fig. 6e–f), we identify two leading centers for the LCPs. One center is located in southern Asia, a similar region to the ASM dehydration center but displaced slightly southeastward. The other, more significant center is near the NAM itself, which is likely the main contributor to the increase in reconstructed water vapor concentrations in the NAM. This suggests that the increase in reconstructed water vapor concentrations in the NAM region is primarily influenced by local tropopause temperatures, with additional moisture contributions from transport from southern Asia. In the trajectory simulations, the average backward period required to trace observed air parcels back to their LCPs for the NAM is ~45 days (Fig. S2c–d). This indicates that the temperatures used to reconstruct the water vapor at those LCPs are partially from June or even earlier, which are lower than the temperatures in August, leading to lower reconstructions.

The locations of LCPs for the tropics (Fig. 5a–b) resemble an ensemble of those found in the ASM and NAM, suggesting that dehydration predominantly occurs near the monsoon regions. Additionally, the PDFs for the tropics (Fig. 6a–b) show that LCPs are highly concentrated in southern Asia, even when considering only the top 10%, reinforcing the significance of southern Asia as a major dehydration center of the monsoon regions.

## 3.3 Lagrangian reconstruction and convection

325

330

335

340

350

We further investigate the relation between the dry bias in the reconstructions and convection as a potential moistening process. Therefore, we follow recent studies (e.g., Randel et al., 2015; Peña-Ortiz et al., 2024) and use OLR as a proxy for convection intensity, with high OLR values corresponding to weak convection and low OLR values corresponding to strong convection.

Note that while OLR is a commonly used proxy, it has limitations—it primarily captures cold cloud tops and may miss warm-topped or thin convection, leading to potential biases in certain regions or conditions (e.g., Liu et al., 2007). Randel et al. (2015) used MLS observations from May to September (2005–2013) to obtain time series of UTLS (100 hPa) water vapor concentrations in the ASM, separating specific wet and dry phases to reveal the corresponding anomalous convection patterns. Their findings indicate that convection exhibits a west-east dipole structure over the whole ASM region. The strong convection over the eastern part of the dipole (20–30°N, 80–110°E) corresponds to a dry phase in the ASM UTLS (i.e. low UTLS water vapor mixing ratios over the whole ASM) and vice versa. We conduct a similar analysis to derive OLR indices and then composite water vapor concentrations within the entire ASM region (15–35°N, 60–140°E) for observations from SAGE III/ISS and the reconstructions. Two OLR indices are defined according to the dipole structure: an OLR-West index quantifies convection intensity in the western part, while an OLR-East index quantifies convection intensity in the eastern part of the ASM (Sect. 2.2). These indices are used to select days with relatively weak convection (OLR  $\geq$  1.5 standard deviations) and strong convection (OLR  $\leq$  -1.5 standard deviations). The west-east shifts in convection, as reflected in these OLR indices, may be related to different modes of the ASM anticyclone (Honomichl and Pan, 2020).

Figure 7 presents water vapor observations and reconstructions averaged over the 0–10 days following strong and weak convection events. The composites for convection intensity in the eastern part of the ASM reveal that observed water vapor mixing ratios are drier for strong-convection days than those composited for weak-convection days below 17.5 km (Fig. 7a). This drying effect of convection is weak within the stratosphere at 17.5 km (-0.21 ppmv) but increases to -6.6 ppmv at 15.5 km within troposphere. Conversely, the composites for convection intensity in the western part of the ASM show the opposite trend: composited water vapor concentrations for strong-convection periods are higher than those for weak-convection periods below 17.5 km (Fig. 7b). Our results are consistent with Randel et al. (2015), demonstrating that strong convection in the eastern part of the ASM is associated with a dry UTLS, whereas a westward shift of strong convection is associated with a moist UTLS.

The right panels of Fig. 7 display the reconstructed water vapor profiles. Below the lapse rate tropopause (yellow dashed lines), the reconstructions show an insignificant response to changes in convection intensity compared to the observations. This finding suggests that the reconstruction is not capable of catching the influence of the west-east shift of convection in the ASM region. These differences between the reconstruction and observations concerning the effect of convection in the ASM region highlight a key limitation of the simple Lagrangian water vapor reconstruction method: while it effectively represents large-scale dehydration and transport processes, it struggles to accurately represent convective moistening and drying, along with localized processes in the upper troposphere. This limitation is also evident in Fig. 2b, where the reconstructions exhibit increasing dry biases from less than 2 ppmv in the stratosphere (above 17.5 km) to a maximum of 5 ppmv in the troposphere (15.5 km).

Figure 8 further examines the relation between convection intensity (based on the OLR-indices defined above) and the biases in reconstructed water vapor concentrations at 16.5 km based on SAGE III/ISS. Overall, convection in the eastern part of the ASM is stronger (OLR 200–230 W/m²) than in the western part of the ASM (OLR 240–280 W/m²). However, no significant correlation of the reconstruction bias to convection in the eastern monsoon region is found (Fig. 8a), suggesting

that eastern convection does not significantly impact the reconstruction performance. In contrast, convection in the western monsoon region exhibits a significant correlation with the reconstruction bias, with a correlation coefficient of 0.73 (Fig. 8b). Despite being weaker than eastern convection, western convection has a stronger influence on the biases, leading to increased dry biases in the reconstructions following periods of strong convection. This pattern is also evident when comparing Fig. 7b and 7d. In addition, the correlation between reconstructed biases and convection intensity in the western monsoon region (OLR-West index) varies with altitude, with correlation coefficients of 0.47, 0.73\* (with a star indicating statistical significance at the 95% confidence level based on the Student's t-test), 0.46, and 0.24 from 16.0 km to 17.5 km (with 0.5 km interval). With the exception of 16.5 km, the correlations at other levels do not pass the significance test. The correlation maximum at 16.5 km highlights the relevance of convection-driven processes near the tropopause. We attribute this altitude-dependent behavior to different atmospheric regimes: at and below 16.5 km, convection has a stronger influence, whereas above 17.0 km, the Lagrangian reconstruction becomes less sensitive to convection and is dominated by large-scale transport and the trajectory history of air parcels.

## 4 Discussion

405

410

415

420

As shown in Fig. 1 and Fig. 2, the reconstructions exhibit a consistent dry bias (~1.5 ppmv) above the cold point tropopause in both the ASM region and throughout the broader tropics. A similar dry bias has been reported by Liu et al. (2010), who suggested that incorporating cloud microphysical processes could significantly reduce this bias by relaxing the assumption of instantaneous dehydration to the saturation mixing ratio. Similarly, Schoeberl et al. (2013) implemented a Lagrangian cloud model that simulates the conversion of excess water vapor to ice, and setting parcels to saturation within convection zones. They showed that including such simplified Lagrangian cloud model improves agreement with MLS observations. Also other studies have shown that a simple allowance for supersaturation at LCPs can substantially reduce the dry bias (Schiller et al., 2009; Ploeger et al., 2011). However, while effective, this approach remains a simplified representation of the complex microphysical processes that influence dehydration efficiency, as well as of other small-scale processes like turbulence and mixing (Poshyvailo et al., 2018). Such underrepresented processes can contribute to the dry bias in our reconstructions.

While the simplified Lagrangian method performs well in reconstructing the moist anomaly in the ASM, it struggles with representing the moisture budget in the NAM, suggesting that different mechanisms may be at play in this region. Previous studies indicate that, in boreal summer, the ASM is characterized by a strong anticyclonic circulation at 100 hPa, along with a smaller, approximately symmetric anticyclone in the Southern Hemisphere subtropics, which can be explained by the dynamical structure of the Gill response (Park et al., 2007). In contrast, the geopotential height over North America at 100 hPa exhibits no such structure, highlighting a fundamental difference between the NAM and ASM from a large-scale circulation perspective. Also, studies by Smith et al. (2017) and O'Neill et al. (2021) show that frequent deep convection over North America and particularly intense convective events, can transport water vapor into the lower stratosphere. These findings suggest that deep, potentially overshooting convection might play a more crucial role in the UTLS water vapor budget in the NAM compared to other regions and may be the primary driver of the large biases observed in Lagrangian reconstructions.

Additionally, as suggested by our trajectory simulation results, long-range transport from southern Asia to the NAM region appears to significantly influence NAM water vapor concentrations. On the one hand, the significant fraction of air masses experiencing dehydration over southern Asia before reaching North America implicates the dominant role of the Asian monsoon in controlling the moisture entering the stratosphere during boreal summer, which is consistent with previous studies (Fueglistaler et al., 2004; Ploeger et al., 2013). On the other hand, the limited performance of the reconstruction for the NAM may be attributed to errors in ERA5 winds, which can introduce biases in transport modeling, and diabatic heating rates. Additionally, the presence of multiple, competing mechanisms within convection events may further complicate the accurate representation of long-range transport in models (Homeyer et al., 2024).

Moreover, previous studies have shown that trajectories computed with 6-hourly reanalysis data exhibit transport errors and warm biases of cold point tropopause compared to those calculated with higher temporal resolution (1-hourly) data (Pisso et al., 2010; Bourguet and Linz, 2022). These biases could lead to inaccuracies in simulating dehydration processes and ultimately impact the reconstructed water vapor distribution. Investigating additional tracers originating from Asia could help assess whether long-range transport from Asia to the NAM region and its remote influence on NAM water vapor levels are accurately captured in current trajectory-based reconstructions.

#### 5 Conclusions

425

430

435

440

445

450

455

This study investigates the performance of Lagrangian reconstructions of UTLS water vapor in the boreal summer monsoons over Asia and North America. The reconstructed water vapor fields are evaluated using SAGE III/ISS and MLS observations, with SAGE III/ISS providing higher vertical resolution and revealing finer-scale structures in the UTLS. Our results demonstrate the effectiveness of the Lagrangian method in capturing tropical UTLS water vapor variations and structures, with improved performance from the tropopause upwards.

Overall, the Lagrangian approach, including the temperature history of air masses, is found to be equally effective in reconstructing water vapor mixing ratios in the Asian monsoon as in the deep tropics. Given that most air parcels undergo dehydration in the southern vicinity of the ASM, we conclude that UTLS water vapor concentrations in the ASM are largely governed by large-scale transport through the cold tropopause in this region. A systematic dry bias in reconstructions in the ASM of approximately 1.5 ppmv is similar to dry biases found previously for lower stratospheric water vapor in the deep tropics. Nevertheless, the Lagrangian reconstruction reproduces the anomalies of stratospheric water vapor mixing ratios in the ASM well and captures more than two-thirds of the observed moist anomalies. Reconstructions using larger trajectory ensembles for each satellite observation point show significantly better performance compared to reconstructions based on smaller ensembles.

Conversely, the Lagrangian method fails to reproduce the observed moistening in the NAM region. The ERA5-driven trajectory simulations suggest that while the highest UTLS water vapor concentrations in the NAM are primarily controlled by local tropopause temperatures over America, most air masses in the NAM region are remotely influenced by long-range transport from southern Asia and the associated tropopause temperatures there. We hypothesize that the failure of the water vapor recon-

struction in the NAM UTLS is likely due to an underestimation of local moistening processes such as deep convection and ice injection, which are not explicitly included in the reconstruction method. Additionally, errors in the cross-Pacific long-range transport could be another factor affecting the particularly large dry bias in the NAM reconstructions.

460

465

Finally, based on analyses of convective variability, using outgoing longwave radiation as an indicator of convection, we assessed the impact of convection on UTLS water vapor variability and on the bias in the Lagrangian reconstructions. Based on observations from SAGE III/ISS we can confirm the findings of Randel et al. (2015) which show that strong convection in the eastern part of the ASM leads to UTLS drying, whereas a westward shift of convection results in UTLS moistening. Correlation analyses reveal that the biases in Lagrangian reconstructions are significantly linked to the intensity of convection in the western region of the ASM, with stronger convection associated with increased dry biases. In contrast, no clear influence on the reconstruction bias is found for convection in the eastern part of the ASM. Hence, it is likely the underestimated moistening effect of ice injection of convection in the western region of the Asian monsoon which controls the dry bias of Lagrangian reconstructions in the ASM. Investigating similar connections between model dry biases and convective intensity in other regions appears promising for improving simulations of the UTLS moisture budget.

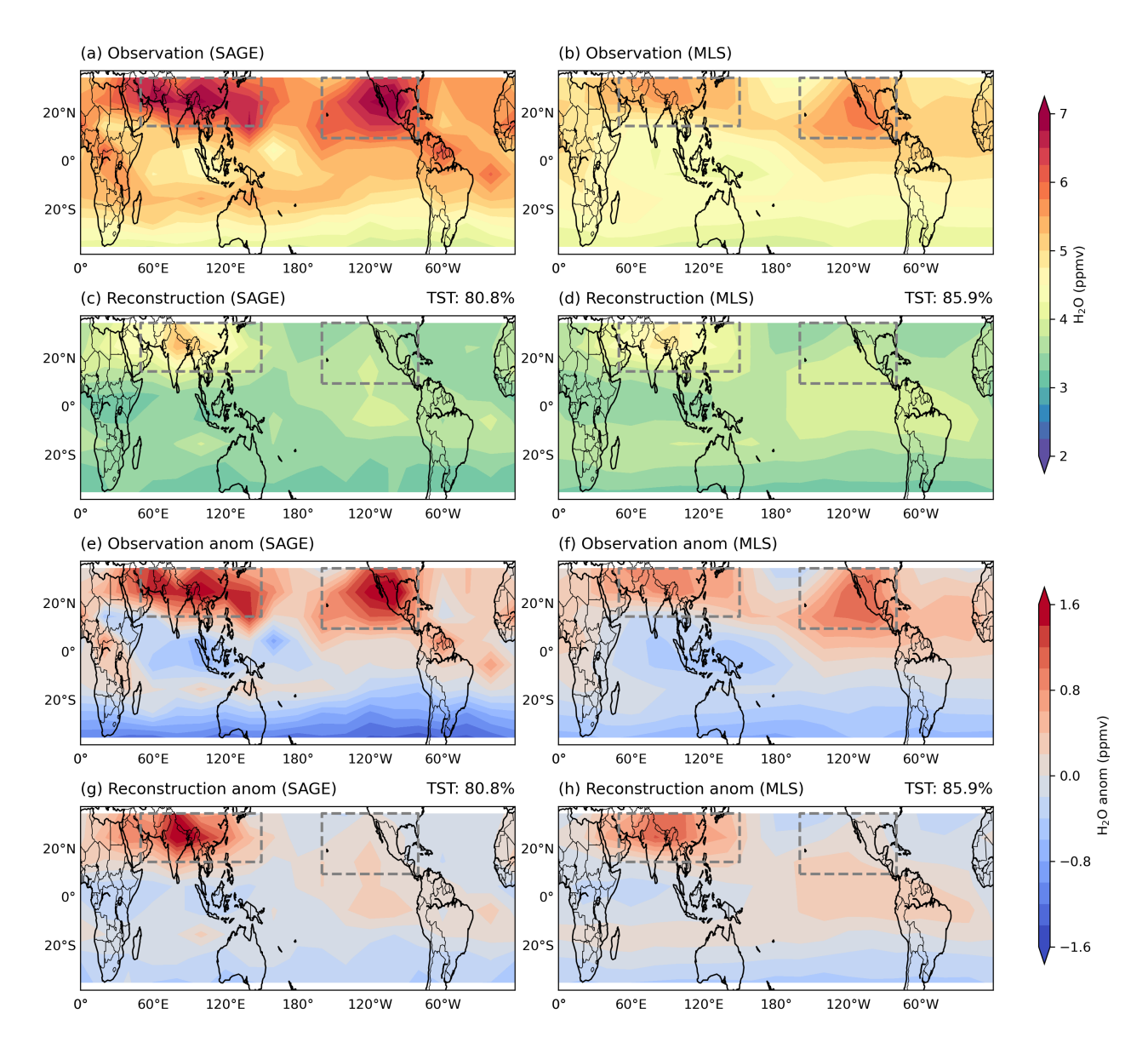


Figure 1. Horizontal distribution of water vapor concentrations and anomalies in August. Observed water vapor  $(H_2O)$  concentrations (a-b), the reconstructed concentrations of Experiment LAG (c-d) and corresponding anomalies (e-h) based on SAGE III/ISS at 16.5 km (left) and MLS at  $\sim 16.3$  km (right). The anomalies are calculated by subtracting the average values of the entire tropics  $(35^{\circ}S \text{ to } 35^{\circ}N)$ . Grey boxes in each subplot show the defined area of ASM  $(15^{\circ}-35^{\circ}N, 50^{\circ}-150^{\circ}E)$  and NAM  $(10^{\circ}-35^{\circ}N, 160^{\circ}-80^{\circ}W)$ . Reconstructions in this figure use both TSTs and non-TSTs, the portions of TST are shown with upper right strings of c-d and g-h.

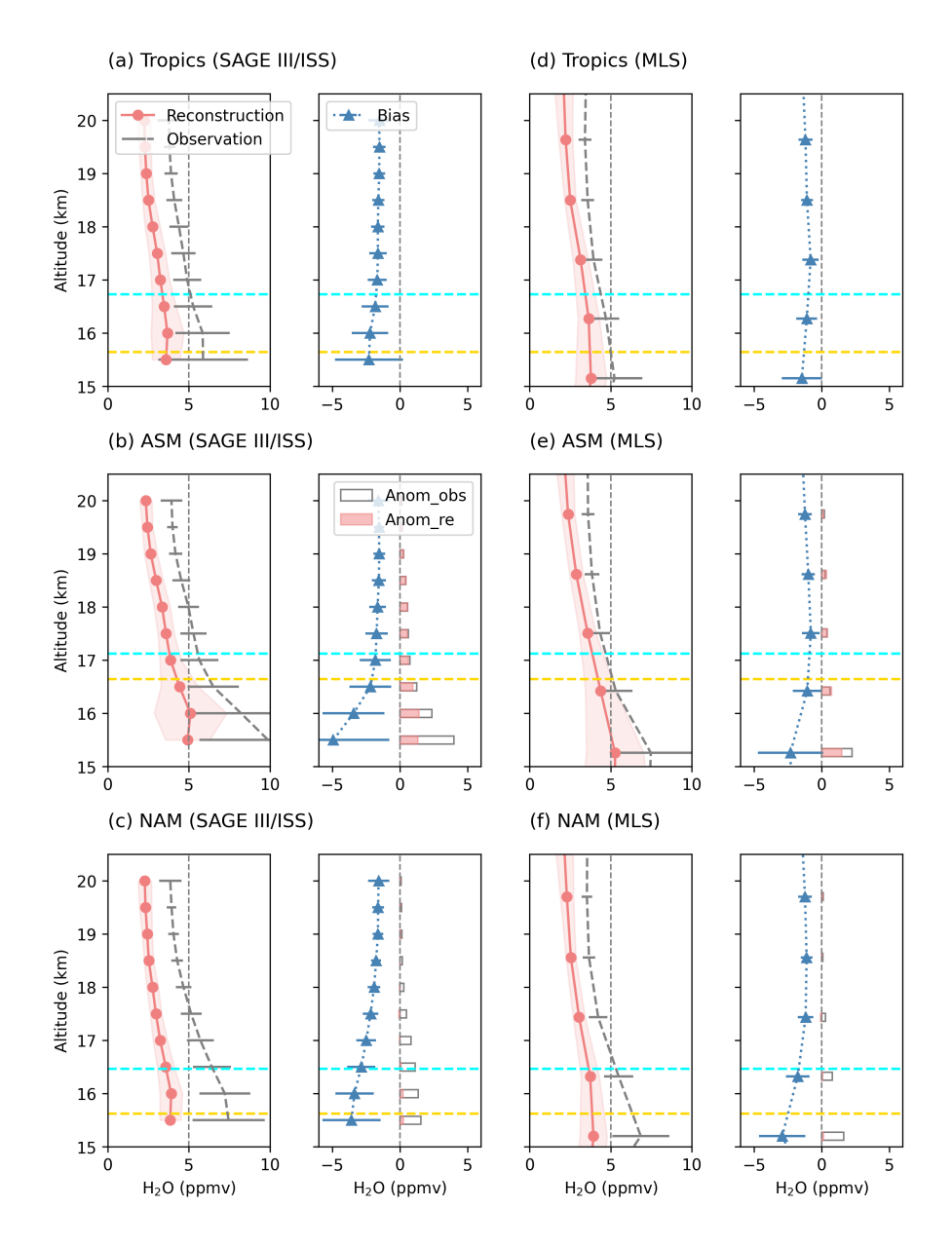
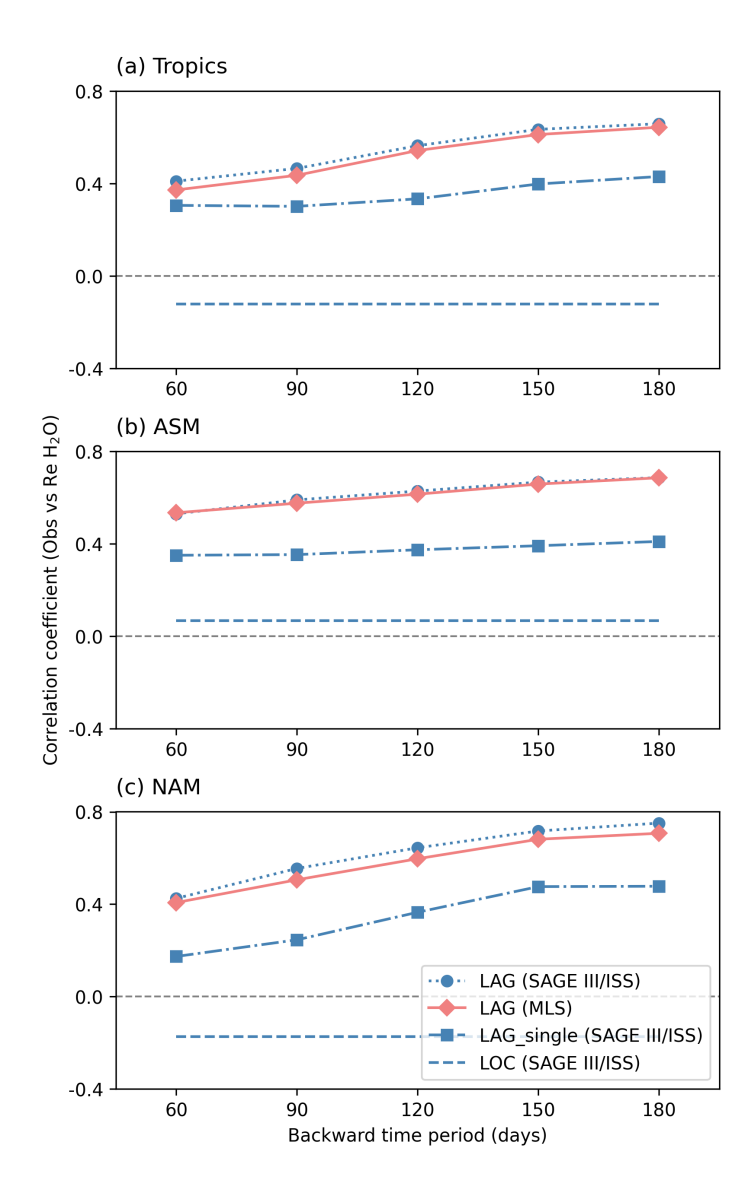
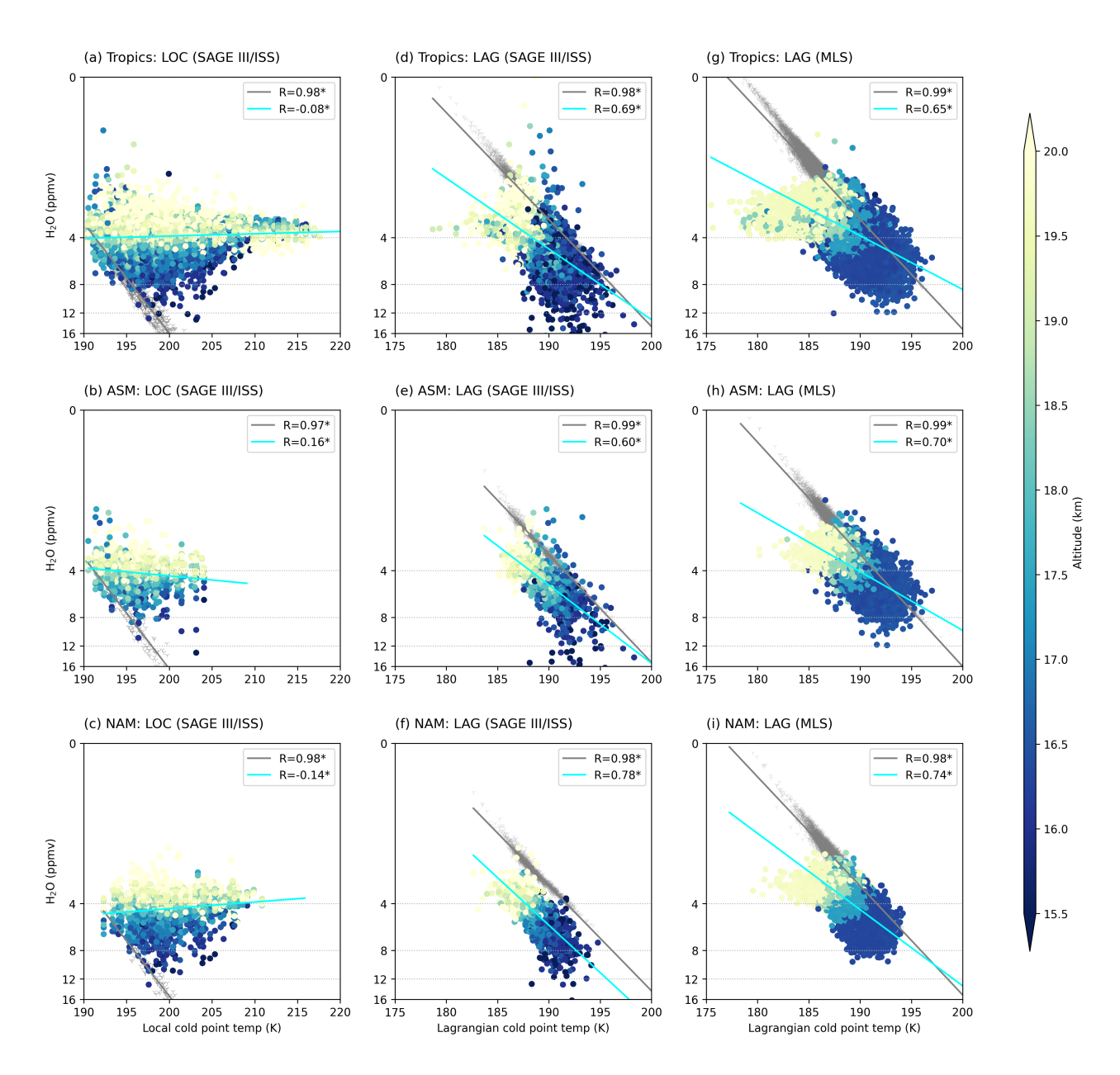


Figure 2. Vertical profiles of water vapor ( $H_2O$ ) concentrations in August. For each subplot, it shows observed water vapor concentrations (grey dotted lines), reconstructed concentrations of Experiment LAG (coral lines, TST-only) and the bias between them (reconstructed values subtract observed values, blue lines). Upper, middle and lower columns show the averaged values in the tropics ( $35^{\circ}S-35^{\circ}N$ ), ASM and NAM, from SAGE III/ISS (left panels) and MLS (right panels). The cyan horizontal dashed lines indicate the position of the climatological cold point tropopause in August, while the yellow horizontal dashed lines represent the lapse rate tropopause defined by WMO. Both tropopauses are derived from ERA5 reanalysis. For the ASM (b, e) and NAM (c, f), the gray bars in the right sub-panels represent the observed anomalies, while the coral bars indicate the reconstructed anomalies. The anomalies are calculated by subtracting the corresponding mean values in the tropics, as shown in (a) and (d).



**Figure 3.** Correlation coefficients between observed and reconstructed water vapor concentrations (TST-only). Upper, middle and lower panels show the correlation coefficients between 15.5–20.0 km within in entire tropics (a), ASM (b) and NAM (c), respectively. Red diamonds represent the results of Experiment LAG based on MLS dataset. Blue crosses, squares and rounds represent the results based on SAGE III/ISS dataset of LOC, LAG\_single and LAG, respectively. The LOC values remain constant as they do not vary with backward time in Lagrangian experiments.



**Figure 4.** Scatters of water vapor (H<sub>2</sub>O) concentrations (TST-only) vs cold point temperatures. Left: water vapor concentrations from SAGE III/ISS vs local cold point temperatures (Experiment LOC). Middle: water vapor concentrations from SAGE III/ISS vs Lagrangian cold point temperatures (Experiment LAG based on SAGE III/ISS). Right: water vapor concentrations from MLS vs Lagrangian cold point temperatures (Experiment LAG based on MLS). Coloured points indicate the observed water vapor concentrations with the colour showing altitudes of the points. Grey dots represent reconstructed concentrations (saturation). The legends show the correlation coefficients and stars indicate statistical significance at the 95% confidence level based on the Student's t-test.

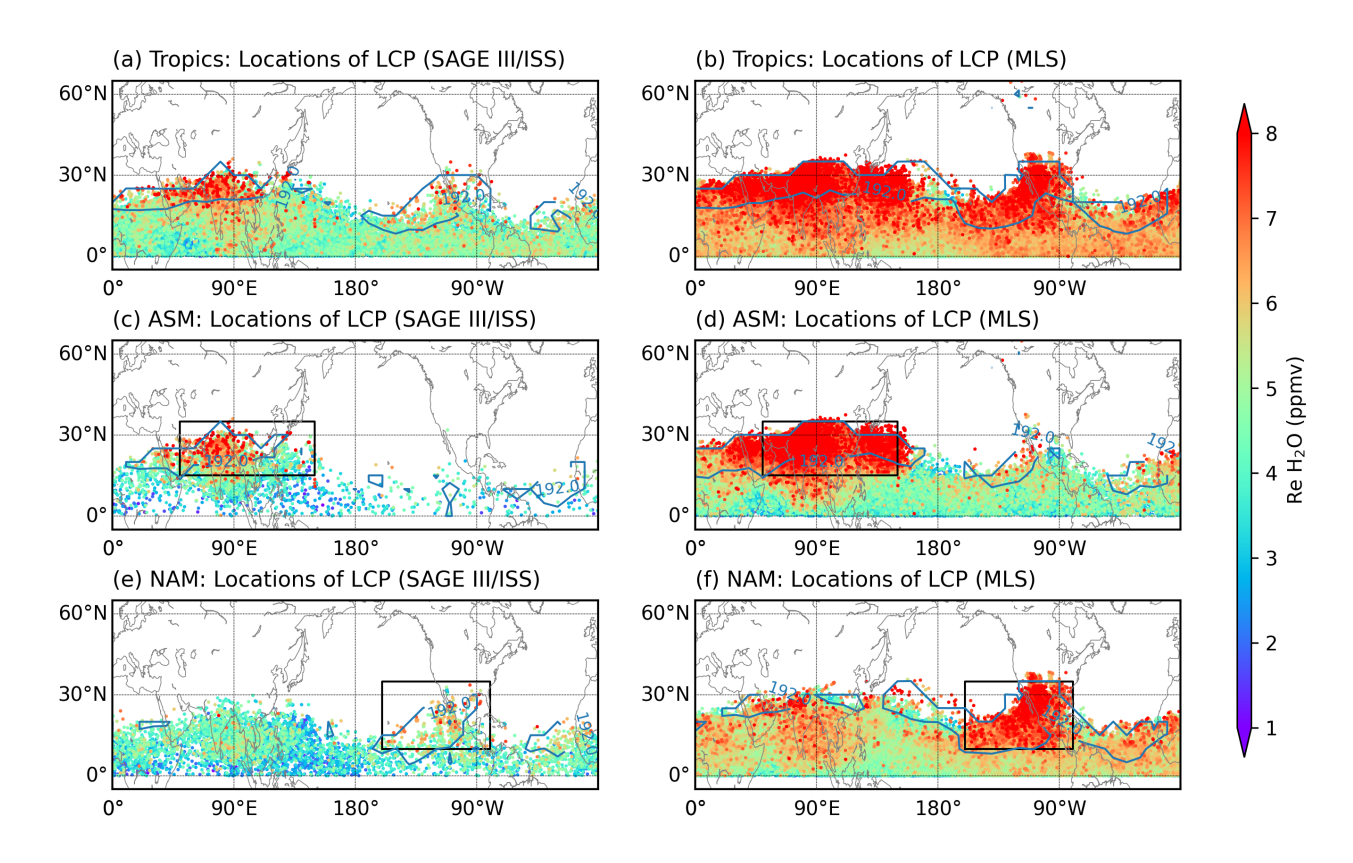
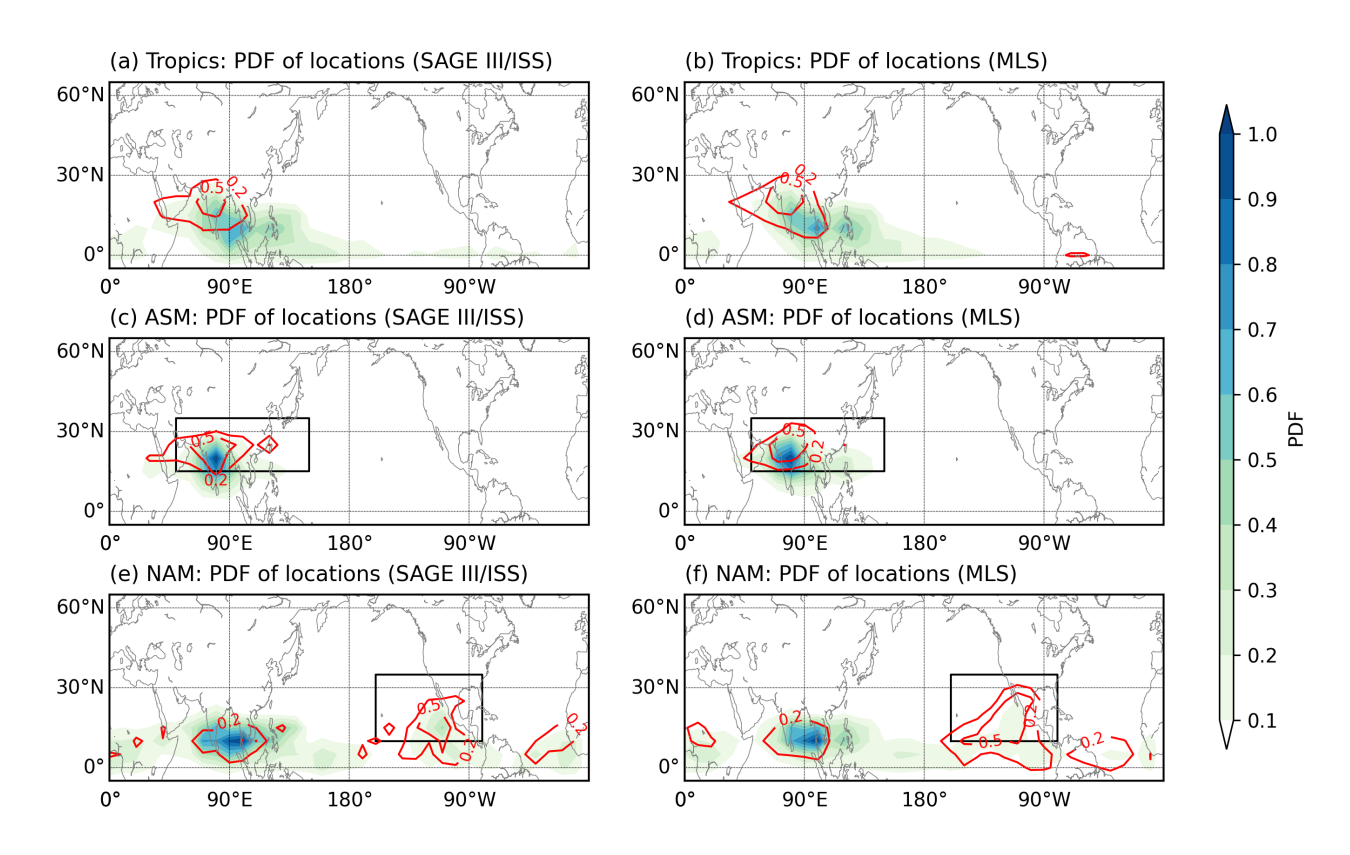


Figure 5. Horizontal distributions of the locations of the Lagrangian cold points (LCPs) used for water vapor ( $H_2O$ ) reconstruction at 16.5 km, derived from Experiment LAG. The locations of the LCPs are shown with colors representing the reconstructed water vapor concentrations, with starting points in the entire tropics (a, b), ASM (c, d) and NAM (e, f). The scatters are plotted in ascending sequence according to the values of reconstructions. The blue contour lines represent a cold point temperatures of 192 K. The left panels (a, c, e) show results based on SAGE III/ISS, while the right panels (b, d, f) show results based on MLS data. The black boxes indicate the original regions of starting points.



**Figure 6.** Probability density functions (PDFs) of the locations of Lagrangian cold points (LCPs) in Fig. 5. The PDFs are presented for the entire tropics (a, b), ASM (c, d) and NAM (e, f), with red contour lines representing the PDFs of the locations with the top 10% highest reconstructed water vapor concentrations. The left panels (a, c, e) show results based on SAGE III/ISS, while the right panels (b, d, f) show results based on MLS data.

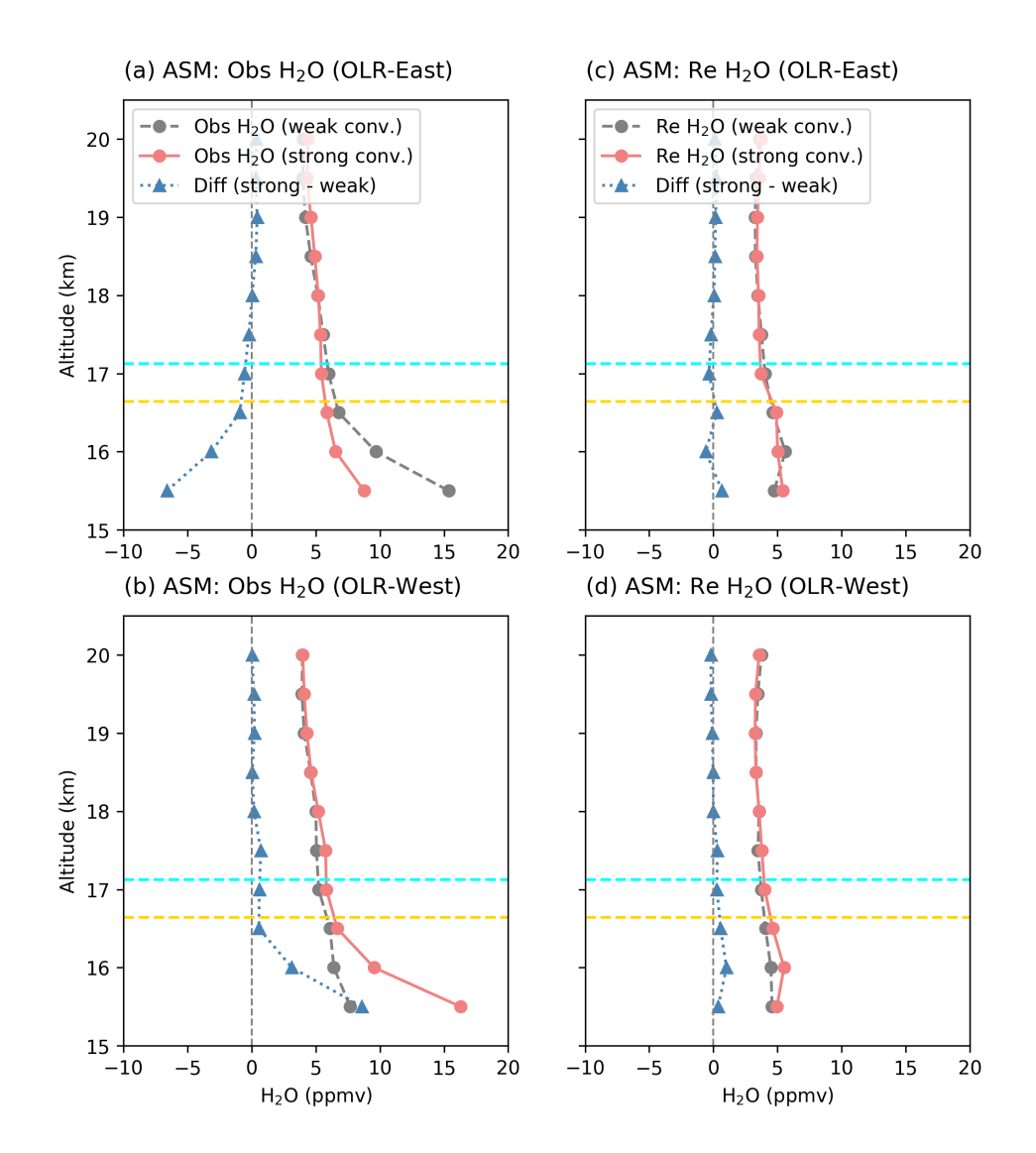
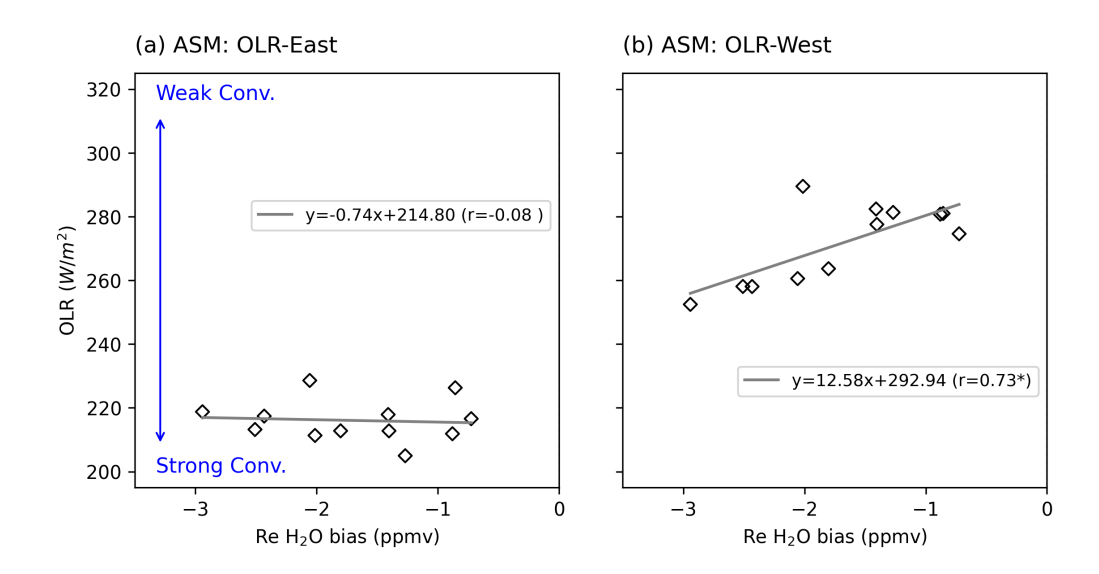


Figure 7. Vertical profiles of water vapor (H<sub>2</sub>O) concentrations under the influence of convection within the ASM region, based on SAGE III/ISS dataset. The left panels show observed water vapor profiles averaged during weak-convection (high-OLR) and strong-convection (low-OLR) days, along with their differences, for OLR-West (a) and OLR-East (b) indices, where OLR is averaged over the western and eastern regions, respectively. Right panels show reconstructed water vapor profiles averaged during weak-convection days, strong-convection days, and their differences, for OLR-West (c) and OLR-East (d) indices. Same as in Fig. 2, the cyan and yellow horizontal dashed lines indicate the positions of the climatological cold point tropopause and lapse rate tropopause in August, respectively.



**Figure 8.** Scatter plots of OLR (convection intensity) versus biases in reconstructed water vapor concentrations (SAGE III/ISS) at 16.5 km for the ASM. Panels (a) and (b) correspond to results using OLR-East and OLR-West, respectively. The biases are half-monthly averaged, while OLR values are first averaged over the 0–10 days preceding each date and then half-monthly averaged. The legends display the regression line equations and correlation coefficients, with a star indicating statistical significance at the 95% confidence level based on the Student's t-test.

Code and data availability. The CLaMS model is available in the CLaMS git database. Detailed information is available at https://clams. icg.kfa-juelich.de/CLaMS/GitLabInstructions. ERA5 reanalysis data are available from the European Centre for Medium-range Weather Forecasts (https://apps.ecmwf.int/data-catalogues/era5/?class=ea), last access: 03 August 2024). The MLS v5.0 water vapor data used in this study are available from NASA's Earthdata website (https://www.earthdata.nasa.gov/learn/find-data/near-real-time/mls). SAGE III/ISS Level 2 Solar Event Species Profiles (HDF5) Version 5.3 data can be accessed through NASA's Atmospheric Science Data Center (https://asdc.larc.nasa.gov/project/SAGE%20III-ISS/g3bssp\_53). The NOAA CPC OLR data are available at (https://psl.noaa.gov/data/gridded/data.cpc\_blended\_olr-2.5deg.html).

Author contributions. H. W. carried out the analysis and wrote the original draft of the manuscript. P. K. and F. P. supervised the research, contributing ideas, guidance, and discussions throughout the study, and assisted with iterative revisions. M. P., M. T., C. P., and N. P. provided comments and suggestions during the manuscript revision. All authors contributed to discussions and final revisions of the paper.

Competing interests. The authors declare no competing interests.

Acknowledgements. The authors would like to express their gratitude to the European Centre for Medium-Range Weather Forecasts (ECMWF) for providing meteorological analysis for this study. We extend our appreciation to Nicole Thomas for her exceptional programming support. Additionally, we thank ChatGPT (https://chat.openai.com, last accessed: March 2025) for their assistance in refining the final text. The CPC Daily Blended Outgoing Longwave Radiation (OLR) - 2.5 degree data was kindly provided by the NOAA PSL, Boulder, Colorado, USA, via their website at https://psl.noaa.gov. FP acknowledges support by the Deutsche Forschungsgemeinschaft (TPChange grant, The Tropopause
 Region in a Changing Atmosphere, DFG TRR 301, Project-ID 428312742).

## References

495

505

- Avery, M., Davis, S., Rosenlof, K., Ye, H., and Dessler, A.: Large anomalies in lower stratospheric water vapour and ice during the 2015-2016 El Ninõ, Nature Geoscience, 10, 405–409, https://doi.org/10.1038/ngeo2961, cited By 67, 2017.
- Bannister, R., O'Neill, A., Gregory, A., and Nissen, K.: The role of the south-east Asian monsoon and other seasonal features in cre-490 ating the 'tape-recorder' signal in the Unified Model, Quarterly Journal of the Royal Meteorological Society, 130, 1531 – 1554, https://doi.org/10.1256/qj.03.106, cited by: 63, 2004.
  - Bourguet, S. and Linz, M.: The impact of improved spatial and temporal resolution of reanalysis data on Lagrangian studies of the tropical tropopause layer, Atmospheric Chemistry and Physics, 22, 13 325–13 339, https://doi.org/10.5194/acp-22-13325-2022, cited By 6, 2022.
  - Brewer, A.: Evidence for a world circulation provided by the measurements of helium and water vapour distribution in the stratosphere, Ouarterly Journal of the Royal Meteorological Society, 75, 351–363, https://doi.org/10.1002/qi.49707532603, cited By 831, 1949.
  - Cisewski, M., Zawodny, J., Gasbarre, J., Eckman, R., Topiwala, N., Rodriguez-Alvarez, O., Cheek, D., and Hall, S.: The stratospheric aerosol and gas experiment (SAGE III) on the International Space Station (ISS) Mission, in: Sensors, Systems, and Next-Generation Satellites XVIII, vol. 9241, pp. 59–65, SPIE, 2014.
- Clemens, J., Ploeger, F., Konopka, P., Portmann, R., Sprenger, M., and Wernli, H.: Characterization of transport from the Asian summer monsoon anticyclone into the UTLS via shedding of low potential vorticity cutoffs, Atmospheric Chemistry and Physics, 22, 3841 3860, https://doi.org/10.5194/acp-22-3841-2022, cited by: 3; All Open Access, Gold Open Access, Green Open Access, 2022.
  - Davis, S., Damadeo, R., Flittner, D., Rosenlof, K., Park, M., Randel, W., Hall, E., Huber, D., Hurst, D., Jordan, A., Kizer, S., Millan, L., Selkirk, H., Taha, G., Walker, K., and Vömel, H.: Validation of SAGE III/ISS Solar Water Vapor Data With Correlative Satellite and Balloon-Borne Measurements, Journal of Geophysical Research: Atmospheres, 126, https://doi.org/10.1029/2020JD033803, cited by: 11; All Open Access, Bronze Open Access, 2021.
  - Fu, R., Hu, Y., Wright, J. S., Jiang, J. H., Dickinson, R. E., Chen, M., Filipiak, M., Read, W. G., Waters, J. W., and Wu, D. L.: Short circuit of water vapor and polluted air to the global stratosphere by convective transport over the Tibetan Plateau, Proceedings of the National Academy of Sciences of the United States of America, 103, 5664 5669, https://doi.org/10.1073/pnas.0601584103, cited by: 268; All Open Access, Green Open Access, 2006.
- Fueglistaler, S. and Haynes, P.: Control of interannual and longer-term variability of stratospheric water vapor, Journal of Geophysical Research Atmospheres, 110, 1 14, https://doi.org/10.1029/2005JD006019, cited by: 161; All Open Access, Bronze Open Access, 2005.
  - Fueglistaler, S., Wernli, H., and Peter, T.: Tropical troposphere-to-stratosphere transport inferred from trajectory calculations, Journal of Geophysical Research: Atmospheres, 109, D03 108 1–16, https://doi.org/10.1029/2003jd004069, cited by: 162; All Open Access, Bronze Open Access, 2004.
- Fueglistaler, S., Bonazzola, M., Haynes, P. H., and Peter, T.: Stratospheric Water Vapor Predicted From the Lagrangian Temperature History of Air Entering the Stratosphere in the Tropics, Journal of Geophysical Research Atmospheres, https://doi.org/10.1029/2004jd005516, 2005.
  - Fueglistaler, S., Dessler, A., Dunkerton, T., Folkins, I., Fu, Q., and Mote, P.: Tropical tropopause layer, Reviews of Geophysics, 47, https://doi.org/10.1029/2008RG000267, cited by: 743; All Open Access, Bronze Open Access, 2009.
- Hasebe, F. and Noguchi, T.: A Lagrangian description on the troposphere-to-stratosphere transport changes associated with the stratospheric water drop around the year 2000, Atmospheric Chemistry and Physics, 16, 4235 4249, https://doi.org/10.5194/acp-16-4235-2016, cited by: 5; All Open Access, Gold Open Access, Green Open Access, 2016.

- Haynes, P. and Anglade, J.: The vertical-scale cascade in atmospheric tracers due to large-scale differential advection, Journal of the Atmospheric Sciences, 54, 1121 1136, https://doi.org/10.1175/1520-0469(1997)054<1121:TVSCIA>2.0.CO;2, cited by: 125; All Open Access, Bronze Open Access, 1997.
  - Hersbach, H., Bell, B., Berrisford, P., Hirahara, S., Horányi, A., Muñoz-Sabater, J., Nicolas, J., Peubey, C., Radu, R., Schepers, D., Simmons, A., Soci, C., Abdalla, S., Abellan, X., Balsamo, G., Bechtold, P., Biavati, G., Bidlot, J., Bonavita, M., De Chiara, G., Dahlgren, P., Dee, D., Diamantakis, M., Dragani, R., Flemming, J., Forbes, R., Fuentes, M., Geer, A., Haimberger, L., Healy, S., Hogan, R. J., Hólm, E., Janisková, M., Keeley, S., Laloyaux, P., Lopez, P., Lupu, C., Radnoti, G., de Rosnay, P., Rozum, I., Vamborg, F., Villaume, S., and Thépaut, J.-N.: The ERA5 global reanalysis, Quarterly Journal of the Royal Meteorological Society, 146, 1999 2049,
- laume, S., and Thépaut, J.-N.: The ERA5 global reanalysis, Quarterly Journal of the Royal Meteorological Society, 146, 1999 2049 https://doi.org/10.1002/qj.3803, cited by: 11844; All Open Access, Hybrid Gold Open Access, 2020.
  - Holton, J. R. and Gettelman, A.: Horizontal transport and the dehydration of the stratosphere, Geophysical Research Letters, 28, 2799 2802, https://doi.org/10.1029/2001GL013148, cited by: 318, 2001.
- Homeyer, C. R., Smith, J. B., Bedka, K. M., Bowman, K. P., Wilmouth, D. M., Ueyama, R., Dean-Day, J. M., St. Clair, J. M., Hannun,
   R., Hare, J., et al.: Extreme altitudes of stratospheric hydration by midlatitude convection observed during the DCOTSS field campaign,
   Geophysical Research Letters, 50, e2023GL104 914, 2023.
  - Homeyer, C. R., Gordon, A. E., Smith, J. B., Ueyama, R., Wilmouth, D. M., Sayres, D. S., Hare, J., Pandey, A., Hanisco, T. F., Dean-Day, J. M., et al.: Stratospheric hydration processes in tropopause-overshooting convection revealed by tracer-tracer correlations from the DCOTSS field campaign. Journal of Geophysical Research: Atmospheres, 129, e2024JD041 340, 2024.
- Honomichl, S. B. and Pan, L. L.: Transport From the Asian Summer Monsoon Anticyclone Over the Western Pacific, Journal of Geophysical Research: Atmospheres, 125, https://doi.org/10.1029/2019JD032094, cited by: 27, 2020.
  - Jensen, E., Pan, L., Honomichl, S., Diskin, G., Krämer, M., Spelten, N., Günther, G., Hurst, D., Fujiwara, M., Vömel, H., Selkirk, H., Suzuki, J., Schwartz, M., and Smith, J.: Assessment of Observational Evidence for Direct Convective Hydration of the Lower Stratosphere, Journal of Geophysical Research: Atmospheres, 125, https://doi.org/10.1029/2020JD032793, cited By 20, 2020.
- Jorgensen, D. and Lemone, M.: Vertical velocity characteristics of oceanic convection, Journal of the Atmospheric Sciences, 46, 621 640, https://doi.org/10.1175/1520-0469(1989)046<0621:VVCOOC>2.0.CO;2, cited by: 201; All Open Access, Bronze Open Access, 1989.
  - Konopka, P., Tao, M., Von Hobe, M., Hoffmann, L., Kloss, C., Ravegnani, F., Volk, C. M., Lauther, V., Zahn, A., Hoor, P., and Ploeger, F.: Tropospheric transport and unresolved convection: numerical experiments with CLaMS 2.0/MESSy, Geoscientific Model Development, 15, 7471 7487, https://doi.org/10.5194/gmd-15-7471-2022, cited by: 5; All Open Access, Gold Open Access, Green Open Access, 2022.
- Konopka, P., Rolf, C., Von Hobe, M., Khaykin, S. M., Clouser, B., Moyer, E., Ravegnani, F., D'Amato, F., Viciani, S., Spelten, N., Afchine, A., Krämer, M., Stroh, F., and Ploeger, F.: The dehydration carousel of stratospheric water vapor in the Asian summer monsoon anticyclone, Atmospheric Chemistry and Physics, 23, 12 935 12 947, https://doi.org/10.5194/acp-23-12935-2023, 2023.
  - Kumar, V. and Krishnan, R.: On the association between the Indian summer monsoon and the tropical cyclone activity over northwest Pacific, Current science, pp. 602–612, 2005.
- Lambert, A., Werner, F., Read, W. G., Froidevaux, L., Schwartz, M. J., Wagner, P. A., Daffer, W. H., Livesey, N. J., Pumphrey, H. C., Manney, G. L., et al.: Version 5 Level-2 Near-Real-Time Data User Guide, Tech. rep., Tech. Rep. JPL D-48439 d, Jet Propulsion Laboratory, California Institute of ..., 2017.

560

Liu, C., Zipser, E. J., and Nesbitt, S. W.: Global distribution of tropical deep convection: Different perspectives from TRMM infrared and radar data, Journal of Climate, 20, 489 – 503, https://doi.org/10.1175/JCLI4023.1, cited by: 190; All Open Access, Bronze Open Access, Green Open Access, 2007.

- Liu, Y., Fueglistaler, S., and Haynes, P.: Advection-condensation paradigm for stratospheric water vapor, Journal of Geophysical Research Atmospheres, 115, https://doi.org/10.1029/2010JD014352, cited by: 62, 2010.
- Livesey, N., Read, W., Wagner, L., Froidevaux, P., Lambert, A., Manney, G., Millán Valle, L., Pumphrey, H., Santee, M., Schwartz, M., et al.: Version 4.2 x Level 2 and 3 data quality and description document (Tech. Rep. No. JPL D-33509 Rev. E), Jet Propulsion Laboratory, 2020.
- McKenna, D. S., Grooß, J.-U., Günther, G., Konopka, P., Müller, R., Carver, G., and Sasano, Y.: A new Chemical Lagrangian Model of the Stratosphere (CLaMS) 2. Formulation of chemistry scheme and initialization, Journal of Geophysical Research Atmospheres, 107, ACH 4–1 – ACH 4–14, https://doi.org/10.1029/2000JD000113, cited by: 116, 2002.
  - Mote, P. W., Rosenlof, K. H., Holton, J. R., Harwood, R. S., and Waters, J. W.: Seasonal variations of water vapor in the tropical lower stratosphere, Geophysical Research Letters, 22, 1093 1096, https://doi.org/10.1029/95GL01234, cited by: 83, 1995.
- Mote, P. W., Rosenlof, K. H., McIntyre, M. E., Carr, E. S., Gille, J. C., Holton, J. R., Kinnersley, J. S., Pumphrey, H. C., Russell III, J. M., and Waters, J. W.: An atmospheric tape recorder: The imprint of tropical tropopause temperatures on stratospheric water vapor, Journal of Geophysical Research Atmospheres, 101, 3989 4006, https://doi.org/10.1029/95JD03422, cited by: 626; All Open Access, Green Open Access, 1996.
- Nützel, M., Podglajen, A., Garny, H., and Ploeger, F.: Quantification of water vapour transport from the Asian monsoon to the stratosphere,

  Atmospheric Chemistry and Physics, 19, 8947 8966, https://doi.org/10.5194/acp-19-8947-2019, cited by: 22; All Open Access, Gold Open Access, 2019.
  - O'Neill, M., Orf, L., Heymsfield, G., and Halbert, K.: Hydraulic jump dynamics above supercell thunderstorms, Science, 373, 1248–1251, https://doi.org/10.1126/science.abh3857, cited By 24, 2021.
- Park, M., Randel, W. J., Gettelman, A., Massie, S. T., and Jiang, J. H.: Transport above the Asian summer monsoon anticyclone inferred from Aura Microwave Limb Sounder tracers, Journal of Geophysical Research Atmospheres, 112, https://doi.org/10.1029/2006JD008294, cited by: 280; All Open Access, Bronze Open Access, Green Open Access, 2007.
  - Park, M., Randel, W. J., Damadeo, R. P., Flittner, D. E., Davis, S. M., Rosenlof, K. H., Livesey, N., Lambert, A., and Read, W.: Near-Global Variability of Stratospheric Water Vapor Observed by SAGE III/ISS, Journal of Geophysical Research: Atmospheres, 126, https://doi.org/10.1029/2020JD034274, cited by: 6; All Open Access, Green Open Access, 2021.
- Peña-Ortiz, C., Plaza, N. P., Gallego, D., and Ploeger, F.: Quasi-biennial oscillation modulation of stratospheric water vapour in the Asian monsoon, Atmospheric Chemistry and Physics, 24, 5457 5478, https://doi.org/10.5194/acp-24-5457-2024, cited by: 0, 2024.
  - Pisso, I., Marécal, V., Legras, B., and Berthet, G.: Sensitivity of ensemble Lagrangian reconstructions to assimilated wind time step resolution, Atmospheric Chemistry and Physics, 10, 3155–3162, https://doi.org/10.5194/acp-10-3155-2010, cited By 11, 2010.
  - Plaza, N. P., Podglajen, A., Peña-Ortiz, C., and Ploeger, F.: Processes influencing lower stratospheric water vapour in monsoon anticyclones: insights from Lagrangian modelling, Atmospheric Chemistry and Physics, 21, 9585–9607, 2021.

590

- Ploeger, F., Fueglistaler, S., Grooß, J.-U., Günther, G., Konopka, P., Liu, Y., Uller, R., Ravegnani, F., Schiller, C., Ulanovski, A., and Riese, M.: Insight from ozone and water vapour on transport in the tropical tropopause layer (TTL), Atmospheric Chemistry and Physics, 11, 407–419, https://doi.org/10.5194/acp-11-407-2011, cited By 54, 2011.
- Ploeger, F., Günther, G., Konopka, P., Fueglistaler, S., Müller, R., Hoppe, C., Kunz, A., Spang, R., Grooß, J.-U., and Riese, M.: Horizontal water vapor transport in the lower stratosphere from subtropics to high latitudes during boreal summer, Journal of Geophysical Research Atmospheres, 118, 8111 8127, https://doi.org/10.1002/jgrd.50636, cited by: 98; All Open Access, Green Open Access, 2013.

- Poshyvailo, L., Müller, R., Konopka, P., Günther, G., Riese, M., Podglajen, A., and Ploeger, F.: Sensitivities of modelled water vapour in the lower stratosphere: Temperature uncertainty, effects of horizontal transport and small-scale mixing, Atmospheric Chemistry and Physics, 18, 8505–8527, https://doi.org/10.5194/acp-18-8505-2018, cited By 18, 2018.
- Randel, W. and Park, M.: Diagnosing Observed Stratospheric Water Vapor Relationships to the Cold Point Tropical Tropopause, Journal of Geophysical Research: Atmospheres, 124, 7018–7033, https://doi.org/10.1029/2019JD030648, cited By 50, 2019.
  - Randel, W., Moyer, E., Park, M., Jensen, E., Bernath, P., Walker, K., and Boone, C.: Global variations of HDO and HDO/H2O ratios in the upper troposphere and lower stratosphere derived from ACE-FTS satellite measurements, Journal of Geophysical Research Atmospheres, 117, https://doi.org/10.1029/2011JD016632, cited By 69, 2012.
- Randel, W. J., Wu, F., Oltmans, S. J., Rosenlof, K., and Nedoluha, G. E.: Interannual changes of stratospheric water vapor and correlations with tropical tropopause temperatures, Journal of the Atmospheric Sciences, 61, 2133 2148, https://doi.org/10.1175/1520-0469(2004)061<2133:ICOSWV>2.0.CO;2, cited by: 216; All Open Access, Bronze Open Access, 2004.
  - Randel, W. J., Zhang, K., and Fu, R.: What controls stratospheric water vapor in the NH summer monsoon regions?, JOURNAL OF GEO-PHYSICAL RESEARCH-ATMOSPHERES, 120, 7988–8001, https://doi.org/10.1002/2015JD023622, 2015.
- Read, W., Lambert, A., Bacmeister, J., Cofield, R., Christensen, L., Cuddy, D., Daffer, W., Drouin, B., Fetzer, E., Froidevaux, L., Fuller, R., Herman, R., Jarnot, R., Jiang, J., Jiang, Y., Kelly, K., Knosp, B., Kovalenko, L., Livesey, N., Liu, H.-C., Manney, G., Pickett, H., Pumphrey, H., Rosenlof, K. H., Sabounchi, X., Santee, M., Schwartz, M., Snyder, W., Stek, P., Su, H., Takacs, L., Thurstans, R., Vömel, H., Wagner, P., Waters, J., Webster, C., Weinstock, E., and Wu, D.: Aura Microwave Limb Sounder upper tropospheric and lower stratospheric H2O and relative humidity with respect to ice validation, Journal of Geophysical Research Atmospheres, 112, https://doi.org/10.1029/2007JD008752, cited by: 193; All Open Access, Bronze Open Access, 2007.
  - Riese, M., Ploeger, F., Rap, A., Vogel, B., Konopka, P., Dameris, M., and Forster, P.: Impact of uncertainties in atmospheric mixing on simulated UTLS composition and related radiative effects, JOURNAL OF GEOPHYSICAL RESEARCH-ATMOSPHERES, 117, https://doi.org/10.1029/2012JD017751, 2012.
- Rolf, C., Vogel, B., Hoor, P., Afchine, A., Günther, G., Krämer, M., Müller, R., Müller, S., Spelten, N., and Riese, M.: Water vapor increase in the lower stratosphere of the Northern Hemisphere due to the Asian monsoon anticyclone observed during the TACTS/ESMVal campaigns, Atmospheric Chemistry and Physics, 18, 2973 2983, https://doi.org/10.5194/acp-18-2973-2018, cited by: 23; All Open Access, Gold Open Access, 2018.
  - Schiller, C., Groob, J.-U., Konopka, P., Plöger, F., Silva Dos Santos, F., and Spelten, N.: Hydration and dehydration at the tropical tropopause, Atmospheric Chemistry and Physics, 9, 9647–9660, https://doi.org/10.5194/acp-9-9647-2009, cited By 73, 2009.
- 625 Schoeberl, M. and Dessler, A.: Dehydration of the stratosphere, Atmospheric Chemistry and Physics, 11, 8433 8446, https://doi.org/10.5194/acp-11-8433-2011, cited by: 92; All Open Access, Gold Open Access, Green Open Access, 2011.
  - Schoeberl, M. R., Dessler, A. E., and Wang, T.: Modeling upper tropospheric and lower stratospheric water vapor anomalies, Atmospheric Chemistry and Physics, 13, 7783–7793, https://doi.org/10.5194/acp-13-7783-2013, 2013.
- Schwartz, M. J., Read, W. G., Santee, M. L., Livesey, N. J., Froidevaux, L., Lambert, A., and Manney, G. L.: Convectively injected water vapor in the North American summer lowermost stratosphere, Geophysical Research Letters, 40, 2316 2321, https://doi.org/10.1002/grl.50421, cited by: 70; All Open Access, Bronze Open Access, 2013.
  - Smith, J., Wilmouth, D., Bedka, K., Bowman, K., Homeyer, C., Dykema, J., Sargent, M., Clapp, C., Leroy, S., Sayres, D., Dean-Day, J., Paul Bui, T., and Anderson, J.: A case study of convectively sourced water vapor observed in the overworld stratosphere over the United States, Journal of Geophysical Research: Atmospheres, 122, 9529–9554, https://doi.org/10.1002/2017JD026831, cited By 64, 2017.

Smith, J., Haynes, P., Maycock, A., Butchart, N., and Bushell, A.: Sensitivity of stratospheric water vapour to variability in tropical tropopause temperatures and large-scale transport, Atmospheric Chemistry and Physics, 21, 2469–2489, https://doi.org/10.5194/acp-21-2469-2021, cited By 7, 2021.

640

655

- Solomon, S., Rosenlof, K. H., Portmann, R. W., Daniel, J. S., Davis, S. M., Sanford, T. J., and Plattner, G.-K.: Contributions of Stratospheric Water Vapor to Decadal Changes in the Rate of Global Warming, SCIENCE, 327, 1219–1223, https://doi.org/10.1126/science.1182488, 2010.
- Sonntag, D.: Advancements in the field of hygrometry, Meteorologische Zeitschrift, 3, 51–66, https://doi.org/10.1127/metz/3/1994/51, 1994. Tao, M., Konopka, P., Wright, J. S., Liu, Y., Bian, J., Davis, S. M., Jia, Y., and Ploeger, F.: Multi-decadal variability controls short-term stratospheric water vapor trends, Communications Earth and Environment, 4, https://doi.org/10.1038/s43247-023-01094-9, cited by: 2; All Open Access, Gold Open Access, 2023.
- 645 Ueyama, R., Jensen, E., Pfister, L., Krämer, M., Afchine, A., and Schoeberl, M.: Impact of Convectively Detrained Ice Crystals on the Humidity of the Tropical Tropopause Layer in Boreal Winter, Journal of Geophysical Research: Atmospheres, 125, https://doi.org/10.1029/2020JD032894, cited By 9, 2020.
  - Ueyama, R., Schoeberl, M., Jensen, E., Pfister, L., Park, M., and Ryoo, J.-M.: Convective Impact on the Global Lower Stratospheric Water Vapor Budget, Journal of Geophysical Research: Atmospheres, 128, https://doi.org/10.1029/2022JD037135, cited By 8, 2023.
- Vogel, B., Müller, R., Günther, G., Spang, R., Hanumanthu, S., Li, D., Riese, M., and Stiller, G.: Lagrangian simulations of the transport of young air masses to the top of the Asian monsoon anticyclone and into the tropical pipe, Atmospheric Chemistry and Physics, 19, 6007–6034, https://doi.org/10.5194/acp-19-6007-2019, cited By 64, 2019.
  - Waters, J. W., Froidevaux, L., Harwood, R. S., Jarnot, R. F., Pickett, H. M., Read, W. G., Siegel, P. H., Cofield, R. E., Filipiak, M. J., Flower, D. A., et al.: The earth observing system microwave limb sounder (EOS MLS) on the Aura satellite, IEEE transactions on geoscience and remote sensing, 44, 1075–1092, 2006.
  - Wright, C. and Gille, J.: HIRDLS observations of gravity wave momentum fluxes over the monsoon regions, Journal of Geophysical Research Atmospheres, 116, https://doi.org/10.1029/2011JD015725, cited by: 35, 2011.
- Yu, W., Dessler, A. E., Park, M., and Jensen, E. J.: Influence of convection on stratospheric water vapor in the North American monsoon region, Atmospheric Chemistry and Physics, 20, 12 153 12 161, https://doi.org/10.5194/acp-20-12153-2020, cited by: 12; All Open Access, Gold Open Access, Green Open Access, 2020.